Remote Sensing of Environment 315 (2024) 114402

Contents lists available at ScienceDirect

Remote Sensing of Environment

journal homepage: www.elsevier.com/locate/rse

DRMAT: A multivariate algorithm for detecting breakpoints in multispectral time series

Yang Li [a,b,*], Michael A. Wulder [c], Zhe Zhu [d], Jan Verbesselt [e], Dainius Masiliūnas [e], Yanlan Liu [b,f], Gil Bohrer [a,g], Yongyang Cai [h], Yuyu Zhou [i,j], Zhaowei Ding [k,l], Kaiguang Zhao [a,b,*]

[a] Environmental Science Graduate Program, The Ohio State University, Columbus, OH 43210, USA
[b] School of Environment and Natural Resources, The Ohio State University, Columbus, OH 43210, USA
[c] Canadian Forest Service (Pacific Forestry Centre), Natural Resources Canada, Victoria, British Columbia, Canada
[d] Department of Natural Resources and the Environment, University of Connecticut, Storrs, CT 06269, USA
[e] Laboratory of Geo-Information Science and Remote Sensing, Wageningen University and Research, Droevendaalsesteeg 3, 6708, PB, Wageningen, the Netherlands
[f] School of Earth Sciences, The Ohio State University, Columbus, OH 43210, USA
[g] Department of Civil, Environmental and Geodetic Engineering, The Ohio State University, Columbus, OH 43210, USA
[h] Department of Agricultural, Environmental, and Development Economics, The Ohio State University, Columbus, OH 43210, USA
[i] Institute for Climate and Carbon Neutrality, The University of Hong Kong, Hong Kong SAR 999077, China
[j] Department of Geography, The University of Hong Kong, 999077, Hong Kong, China
[k] Natural Capital Project, Stanford University, Stanford, CA 94305, USA
[l] The Woods Institute for the Environment, Stanford University, Stanford, CA 94305, USA

ARTICLE INFO

Editor: Marie Weiss

Keywords:
Multivariate analysis
Multispectral bands
Change detection
Time series
Landsat

ABSTRACT

Ecosystem dynamics and ecological disturbances manifest as breakpoints in long-term multispectral remote sensing time series. Typically, these breakpoints are captured using univariate methods applied individually to each band, with subsequent integration of the results. However, multivariate analysis provides a promising way to fully incorporate the multispectral bands into breakpoints detection methods, but it has been rarely applied in monitoring ecosystem dynamics and detecting ecological disturbances. In this research, we developed a multivariate algorithm, named breakpoints-Detection algoRithm using MultivAriate Time series (DRMAT). DRMAT can fully use multispectral bands simultaneously with the consideration of the inter-correlation among bands. It decomposes a multivariate time series into trend, seasonality, and noise, iteratively segmenting the detrended/de-seasonalized signals. We quantitatively evaluated DRMAT using both simulated multivariate data and randomly sampled real-world data, including subtle land cover changes caused by forest disturbances (depletions) and recovery (return of vegetation), as well as subtle changes over a broad range of land cover types. We also qualitatively assessed DRMAT in mapping real-world disturbances. For simulated data with prescribed breakpoints in both trend and seasonality, DRMAT detected breakpoints in trend with an F1 score of 85.5 % and in seasonality with an F1 score of 91.7 %. For real-world data in forested land cover, DRMAT unveiled both disturbances and subsequent recovery with an F1 score of 95.1 % for disturbances and 77.1 % for recovery. It detected disturbances in broader land cover types with an F1 score of 84.0 %. We demonstrated that using all-band data was more accurate than using selected bands in breakpoint detection. The inclusion of vegetation indices as model inputs did not improve accuracy unless the original input bands lacked the specific band information in the vegetation indices. As a multivariate approach, DRMAT leverages the full information in the multispectral data and avoids the necessity of integrating results derived from individual bands.

1. Introduction

The imperative to monitor climate change and ecological disturbances has gained both regional and global prominence, underscoring their pivotal role in contemporary environmental management and stewardship (Bright et al., 2017; Seidl et al., 2017; Zhao and Jackson, 2014). Whether triggered naturally or anthropogenically (e.g., droughts, wildfires, insect infestations, deforestation, and urbanization),

* Corresponding authors at: Environmental Science Graduate Program, The Ohio State University, Columbus, OH 43210, USA.
E-mail addresses: li.10015@osu.edu (Y. Li), zhao.1424@osu.edu (K. Zhao).

https://doi.org/10.1016/j.rse.2024.114402
Received 10 December 2022; Received in revised form 16 July 2024; Accepted 28 August 2024
Available online 11 September 2024

disturbances cause discernible shifts in ecosystem structures and functions, many of which are observable by satellites (Gough et al., 2021; Mildrexler et al., 2007; Hu et al., 2021; Nickerson et al., 2022; Wu et al., 2019). Accurate detection of such changes is crucial for monitoring ecosystem services, tracking carbon storage dynamics, and enhancing land management strategies (Lawler et al., 2014; Quesada et al., 2018).

Remote sensing, with its ability to provide consistent and repeatable measurements, serves as a valuable tool for detecting ecological disturbances (Brooks et al., 2012; Dashti et al., 2024; Verbesselt et al., 2010a). Disturbances are often transient, but their impacts can extend beyond one growth cycle. Therefore, alterations in ecosystem structures, such as biomass and leaf area, can be captured through repeatable remote sensing observations (Hermosilla et al., 2015; Kennedy et al., 2014). Many traditional studies relied on large differences between bi-temporal or multi-temporal data collected over an extended timeframe (e.g., one or multiple years) to identify changes (Coppin et al., 2004; Liu et al., 2018; Lu et al., 2004; Singh, 1989; Zhao et al., 2018). Nowadays, with the increased temporal resolutions achievable (e.g., weekly or monthly intervals) (Li and Roy, 2017; Wulder et al., 2016), more sophisticated approaches have emerged, facilitating the development of time series analysis techniques (Hemati et al., 2021; Zhu, 2017). These algorithms leverage dense stacks of satellite images and track ecosystem changes continuously over time (Frazier et al., 2015; Huang et al., 2010; Masiliūnas et al., 2021a, 2021b; Wulder et al., 2012; Ye et al., 2021; Zhu et al., 2022).

In sync with greater data availability and computing power, many time series algorithms for mapping disturbances have been developed in recent decades. Well-known examples include LandTrendr (Kennedy et al., 2010), BFAST (Verbesselt et al., 2010a), VCT (Huang et al., 2010), CCDC (Zhu and Woodcock, 2014), EWMACD (Brooks et al., 2012; Brooks et al., 2014), C2C (Hermosilla et al., 2016), DBEST (Jamali et al., 2015), BEAST (Zhao et al., 2019), and COLD (Zhu et al., 2020). Methodologically, the core of the existing time series algorithms is breakpoint detection (Schroeder et al., 2017; Zhang et al., 2022). These algorithms decompose satellite time series into trend and/or seasonality, each potentially containing breakpoints. Trend signals are normally modeled as piecewise linear, while seasonality signals are modeled as piecewise harmonics (Brooks et al., 2014; Brooks et al., 2017; Hamunyela et al., 2016; Verbesselt et al., 2010a; Zhao et al., 2019; Zhu and Woodcock, 2014; Zhu et al., 2020). Breakpoints in trend indicate abrupt changes driven by disturbance agents such as forest harvesting, wildfire, and droughts (Kaptué et al., 2015; Vogelmann et al., 2016), whereas breakpoints in seasonality may result from shifts in plant phenology due to climate variables or altered ecosystem composition (Liu and Zhang, 2020; Ma et al., 2019; Rhif et al., 2022; Verbesselt et al., 2010a, 2010b; Zeng et al., 2013; Zhong et al., 2024).

Despite the significant achievements of existing algorithms, several limitations have been identified. Notably, the presence of breakpoints in trend does not necessarily imply the presence of breakpoints in seasonality (Adams et al., 2021; Huang et al., 2010; Li et al., 2022a; Zhao et al., 2019). For example, heatwaves can impose a short-lived stress on vegetation, resulting in a sudden change in the trend without a seasonality shift (Li et al., 2022a). Similarly, fire-burnt forests may exhibit trend breakpoints due to sudden drops in average greenness, but whether seasonal cycles also show breakpoints depends on post-fire species composition recovery (Davies et al., 2022; Fernandes et al., 2013). The opposite is also true: changes in seasonality and phenology do not always indicate a shift in the trend. Even if breakpoints are detected in both trend and seasonality signals, they do not necessarily coincide with each other. Any biases or errors in identifying trend breakpoints will be translated to the biases or errors in identifying seasonal changepoints, and vice versa, which emphasizes the importance of distinguishing between them to enhance overall detection accuracies (Verbesselt et al., 2010a; Zhao et al., 2019). However, many current algorithms, such as DBEST, VCT, and LandTrendr, focus solely on trend data and neglect seasonality. Others, like CCDC and COLD, account for both trend and seasonality but assume that breakpoints occur in both signals at the same time points, which does not always hold true. Our new algorithm development in this study was motivated to avoid this pitfall and explicitly differentiate between trend breakpoints and seasonal breakpoints that can occur asynchronously.

One notable gap in time-series breakpoint detection is the lack of a multivariate algorithm (Huang et al., 2010; Jamali et al., 2015; Verbesselt et al., 2010a; Zhao et al., 2019; Zhu and Woodcock, 2014). This gap is longstanding and particularly striking, especially considering that the majority of satellite data available for ecological and environmental applications is inherently multivariate in nature. Despite the wealth of multivariate data sources, all existing algorithms proposed in the remote sensing community for breakpoint detection—to the best of our knowledge —are inherently univariate. To a lesser extent, the predominant algorithms currently in widespread use, such as LandTrendr, CCDC, COLD, BFAST, and BEAST, also operate as univariate breakpoint detection models. To adapt these univariate algorithms to multivariate or multispectral data, practitioners often employ two strategies, both of which are sub-optimal.

The first strategy for utilizing univariate breakpoint detection algorithms with multispectral data is to select a single spectral band or synthesize multispectral data into a spectral index and then apply the univariate algorithm to the chosen single time series (Chance et al., 2016; Hermosilla et al., 2015; Kennedy et al., 2010). Commonly used indices include the Normalized Difference Vegetation Index (NDVI), the Enhanced Vegetation Index (EVI), the Normalized Difference Moisture Index (NDMI), and the Normalized Burn Ratio (NBR). Another synthesis method is the use of principal component analysis to generate a linear combination of all spectral bands and retain only the first principal component as an index (Hayes and Sader, 2001). Regardless, different bands or indices exhibit varying sensitivities to terrestrial vegetation conditions (Gao et al., 2023; Tewkesbury et al., 2015; Zeng et al., 2023), and the most suitable band or index is typically selected based on empirical evidence or known associations with the desired change features. For example, shortwave infrared (SWIR) bands have been proven reliable for detecting forest disturbances while the blue band has been found less useful (Cohen et al., 2018). When detecting post-disturbance recovery, the near-infrared (NIR) band outperforms others (Negrón-Juárez et al., 2020). Experimental evidence also indicates that SWIR-based indices such as NBR are superior to NDVI or EVI in detecting forest disturbances, particularly those related to fires (Huang et al., 2010; Kennedy et al., 2010). A salient drawback is that, given the different sensitivities of bands and spectral indices to disturbances, applying a time series algorithm using different bands or indices may lead to varied results of detected disturbances (Cohen et al., 2017; Schultz et al., 2016).

The second strategy is to separately apply univariate algorithms to individual spectral bands and then integrate the results into a final list of breakpoints based on certain aggregation rules in an ad-hoc manner (Cohen et al., 2018; Healey et al., 2018; Zhu et al., 2020; Zhu and Woodcock, 2014). The best example of this kind is the CCDC algorithm (Zhu and Woodcock, 2014). This aggregation strategy has been experimentally found to be more useful with better detection accuracies than the first strategy (Potapov et al., 2015; Schultz et al., 2016; Zhu et al., 2020). Given its advantages, practitioners sometimes call detection methods based on the second strategy as “multivariate” algorithms. But technically speaking, they are still univariate and not multivariate, in the same way that we cannot call the running of linear regression multiple times for different response variables as a multivariate linear regression model. Irrespective of the subtleties in technical jargon, the separate application of a univariate algorithm (e.g., BFAST, BEAST, CCDC, and COLD) to multiple spectral bands is theoretically justifiable only if the multispectral bands are statistically independent, which unfortunately is not the case because of strong inter-band correlation. A true multivariate algorithm will model all the time series of different bands jointly, account for inter-band correlation explicitly, estimate the

parameters of interest simultaneously, and provide more reliable and robust estimates. Such benefits of multivariate approaches have been long known in the statistics community (Anderson, 1958) and widely demonstrated in applied fields (Audibert et al., 2020; Jin et al., 2021; Molenaar et al., 2003; Stergiou and Christou, 1996; Swartz et al., 2008; Wang et al., 2022a; Zhang et al., 2019). Despite the theoretical and empirical evidence of multivariate algorithms as well as a clear need from the remote sensing community, such a multivariate time series breakpoint detection algorithm is still lacking—a gap we aim to fill in this study.

This study provides a breakpoints-Detection algoRithm using MultivAriate Time series (DRMAT) to avail upon the full spectral information. Instead of applying an algorithm to multiple input bands separately, it considers all bands simultaneously with the inter-correlation among bands incorporated and the avoidance of integrating final results. The objectives of this study are (1) to decompose multivariate time series and to iteratively detect breakpoints using decomposed signals, and (2) to show its application in ecosystem dynamics and ecological disturbance detection using both simulation data and real-world data.

2. Methods

2.1. Conceptual difference between multivariate approaches and univariate approaches

We first used a example multispectral time series in Fig. 1 to demonstrate the conceptual difference between a multivariate approach and an inherently univariate approach. Here, univariate approaches are defined as methods that can only accept individual time series as the input, despite their ability to combine results from various time series.

Univariate approaches and multivariate approaches differ in three aspects: the number of simultaneous input bands, the incorporation of inter-correlation among these bands, and the need for integrating the final results. Specifically, univariate approaches take only one band as input each time. As long as the input information is put into the model individually, the inter-correlation among input information is not considered, regardless of the richness of the input information (e.g., multiple bands, various vegetation indices). Furthermore, the detected breakpoints using different input bands are not consistent, and different methods used to integrate these results can lead to different breakpoints in the whole signal. As a result, the final breakpoint-or-not decision is heavily dependent on the integration scheme. These potential limitations of univariate approaches can be alleviated by switching to a multivariate approach. The multivariate approach not only leverages the inter-correlation among bands but also eliminates the need to integrate various results by incorporating all the bands simultaneously.

2.2. The DRMAT algorithm

DRMAT shares similarities with the Seasonal-Trend decomposition approach (Cleveland et al., 1990; Verbesselt et al., 2010a), but it can be applied for detecting breakpoints in multivariate time series. Specifically, it detects breakpoints via decomposing the multivariate time series into trend, seasonality and noise signals and segmenting the detrended and de-seasonalized signals iteratively. The source code of the DRMAT is available at https://github.com/YangLiOSU/DRMAT.

2.2.1. Build a multivariate decomposition model with breakpoint information embedded

A multivariate time series $\boldsymbol{Y}_{n\times m}$ includes m bands, each consisting of n observations. We consider such time series to be composed of three components—trend ($\boldsymbol{T}$), seasonality ($\boldsymbol{S}$), and noise ($\boldsymbol{\varepsilon}$) as in Eq. (1):

$$\boldsymbol{Y} = \boldsymbol{T} + \boldsymbol{S} + \boldsymbol{\varepsilon} \tag{1}$$

Based on previous studies (Verbesselt et al., 2010a; Zhao et al., 2019; Zhu et al., 2020), we model the trend $\boldsymbol{T}$ as a piecewise linear function of time with p breakpoints $t^*_{u=1,\ldots,p}$, so the trend $\boldsymbol{T}$ is divided into $p+1$ segments $\left[t^*_u, t^*_{u+1}\right]$ $(u = 0,\ldots,p)$, where t^*_0 and t^*_{p+1} refer to the start and end of the time series (Fig. 2b). Each trend segment $\left[t^*_u, t^*_{u+1}\right]$ is formulated as.

$\widehat{\boldsymbol{T}}_u(t) = \boldsymbol{a}_u + \boldsymbol{b}_u t$ $(u = 0,\ldots,p)$ (2).

The number of breakpoints (p), their timings$\left(t^*_u\right)$, and segment-specific coefficients $(\boldsymbol{a}_u, \boldsymbol{b}_u)$ are recorded in the trend parameters $\boldsymbol{\Theta_T}$:

$$\boldsymbol{\Theta_T} = \{p\} \cup \left\{t^*_u\right\}_{u=1,\ldots,p} \cup \{\boldsymbol{a}_u, \boldsymbol{b}_u\}_{u=0,\ldots,p} \tag{3}$$

The seasonality $\boldsymbol{S}$ is approximated as a piecewise harmonic function of time with q breakpoints $t^*_{v=1,\ldots,q}$, so that $\boldsymbol{S}$ is divided into $q+1$ time

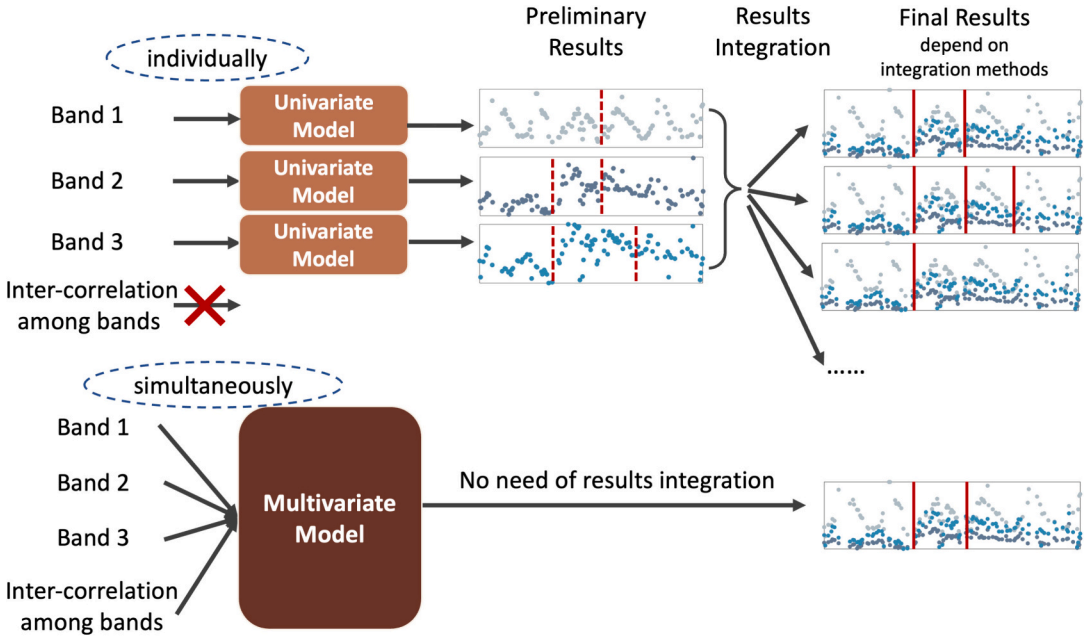

Fig. 1. Illustration of breakpoint detection using a univariate model and a multivariate model.

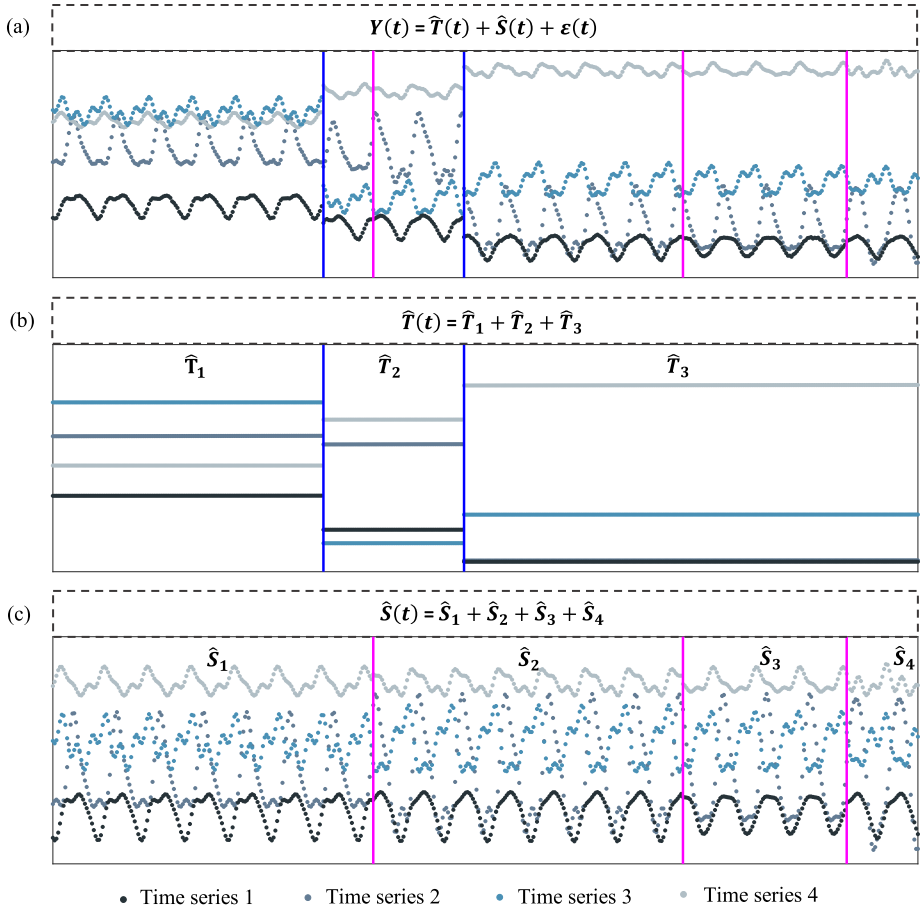

Fig. 2. In the presence of breakpoints in trend and seasonality, a simulated multivariate time series (a) is decomposed into piecewise trend signals (b), piecewise seasonality signals (c), and random noise. Detecting breakpoints in this multispectral time series is achieved by detecting breakpoints in trend and seasonality, respectively. Trend breakpoints (i.e., blue lines) and seasonality breakpoints (i.e., red lines) do not necessarily coincide with each other. (For interpretation of the references to colour in this figure legend, the reader is referred to the web version of this article.)

segments $\left[t_v^*, t_{v+1}^*\right](v = 0, \ldots, q)$, where t_0^* and t_{q+1}^* refer to the start and end of the time series (Fig. 2c). Each seasonality segment $\left[t_v^*, t_{v+1}^*\right]$ is formulated as

$$\hat{\boldsymbol{S}}_v(t) = \sum_{k=1}^{3}\left\{\boldsymbol{a}_{k,v} sin\left(\frac{2\pi kt}{P}\right) + \boldsymbol{b}_{k,v} cos\left(\frac{2\pi kt}{P}\right)\right\} (v = 0, \ldots, q) \quad (4)$$

k is the harmonic order for the vth time segment, P is the period of seasonality. Similarly, the number of breakpoints (q), their timings$\left(t_v^*\right)$, and segment-specific coefficients for all the harmonic terms $\left(\boldsymbol{a}_{k,v}, \boldsymbol{b}_{k,v}\right)$ are recorded in the seasonality parameters $\boldsymbol{\Theta_S}$:

$$\boldsymbol{\Theta_S} = \{q\} \cup \left\{t_v^*\right\}_{v=1,\ldots,q} \cup \left\{\boldsymbol{a}_{k,v}, \boldsymbol{b}_{k,v}\right\}_{k=1,2,3;v=0,\ldots,q} \quad (5)$$

To separate parameters controlling breakpoints from others, we reclassified the model parameters $\{\boldsymbol{\Theta_T}, \boldsymbol{\Theta_S}\}$ into $\{\boldsymbol{L}, \boldsymbol{\beta_L}\}$. $\boldsymbol{L}$ refers to the model structure, including number and timing of the breakpoints in both trend and seasonality.

$$\boldsymbol{L} = \{p\} \cup \left\{t_u^*\right\}_{u=1,\ldots,p} \cup \{q\} \cup \left\{t_v^*\right\}_{v=1,\ldots,q} \quad (6)$$

While $\boldsymbol{\beta_L}$ contains all the parameters that determine the shape of trend and seasonality of each time segment,

$$\boldsymbol{\beta_L} = \{\boldsymbol{a}_u, \boldsymbol{b}_u\}_{u=0,\ldots,p} \cup \left\{\boldsymbol{a}_{k,v}, \boldsymbol{b}_{k,v}\right\}_{k=1,2,3;v=0,\ldots,q} \quad (7)$$

Therefore, the multivariate model to simulate multispectral land surface reflectance is reformulated into Eq. (8):

$$\hat{\boldsymbol{Y}}(t) = \boldsymbol{X}_{\boldsymbol{L}(n\times e)}\boldsymbol{\beta}_{\boldsymbol{L}(e\times m)} \quad (8.1)$$

or

$$\hat{\boldsymbol{Y}}(t) = \boldsymbol{X}_{\boldsymbol{L}(n\times(p+q))}\boldsymbol{\beta}_{\boldsymbol{L}((p+q)\times m)} \quad (8.2)$$

where e is the total number of breakpoints in the multivariate time series if we do not differentiate breakpoints in trend and seasonality. If we do, then p and q refer to the breakpoints in trend and seasonality, respectively.

Next, we describe two model options where one considers simultaneous breakpoints of both trend and seasonality across segments, whereas the other allows the flexibility to differentiate breakpoints in trend versus seasonality thus reducing the dimension of model parameters. For a multivariate model that does not differentiate breakpoints in trend and seasonality (Eq. 8.1), with $e(e = 0, 1, 2, \ldots)$ breakpoints in the multispectral time series, the matrix that describes the model structure (i.e., the design matrix $\boldsymbol{X_L}$) of the multivariate model contains $8 \times (e + 1)$ columns, including $2 \times (e + 1)$ columns describing trend and $6 \times (e + 1)$ columns describing seasonality in the multispectral time series. Here, 2 is the number of coefficients in each trend segment as described in Eq. (2), and 6 is the number of coefficients in each seasonality segment as described in Eq. (4). The parameter matrix $\boldsymbol{\beta_L}$ of the model contains m columns, with each corresponding to one band. Therefore, whenever adding a breakpoint into the model, it adds an extra 8 columns in $\boldsymbol{X_L}$ and 8 rows in $\boldsymbol{\beta_L}$.

For a multivariate model that differentiates the breakpoints in trend

and seasonality (Eq. 8.2), with $(p+q)$ breakpoints (i.e., p breakpoints in trend and q breakpoints in seasonality), the design matrix $\boldsymbol{X_L}$ contains $2\times(p+1)+6\times(q+1)$ columns, where $2\times(p+1)$ columns describing trend and $6\times(q+1)$ columns describing seasonality in the multispectral time series; the parameter matrix $\boldsymbol{\beta_L}$ of the model contains m columns (i.e., m bands) and each column includes $2\times(p+1)+6\times(q+1)$ rows. When adding a trend breakpoint, the multivariate model will be updated with an extra 2 columns in $\boldsymbol{X_L}$ and 2 rows in $\boldsymbol{\beta_L}$; when it is a seasonality breakpoint, it will add an extra 6 columns in $\boldsymbol{X_L}$ and 6 rows in $\boldsymbol{\beta_L}$.

2.2.2. Detecting trend and seasonal breakpoints iteratively

2.2.2.1. Detecting the initial breakpoints with the coupled trend and seasonal signals. We used the Top-Down segmentation algorithm to detect initial breakpoints in the time series. This algorithm traverses the data and identifies breakpoints that minimize the information criteria (Keogh et al., 2004), such as the Akaike information criterion (AIC), the Bayesian information criterion (BIC), and the Hannan-Quinn information criterion (HQC), all of which have been broadly used in model selection (Brewer et al., 2016; Farwell et al., 2021; Gao et al., 2019; Chin et al., 2020). All these three information criteria work by evaluating the model fitting and penalizing the model complexity at the same time. They share the same model fitting evaluation terms but differ in penalty terms (Eq. 9.1, 9.2, and 9.3). AIC penalizes the model complexity with $2\times m\times d$ (Eq. 9.1), where m and d refer to the number of bands and columns of the design matrix $\boldsymbol{X_L}$. By contrast, BIC and HQC penalize model complexity by $ln(n)\times m\times d$ (Eq. 9.2) and $ln(ln(n))\times m\times d$ (Eq. 9.3), respectively, where n denotes the length of the time series.

$$AIC = n\times ln(|\widehat{\Sigma}|)+2\times m\times d \tag{9.1}$$

$$BIC = n\times ln(|\widehat{\Sigma}|)+ln(n)\times m\times d \tag{9.2}$$

$$\mathrm{HQC} = n\times ln(|\widehat{\Sigma}|)+ln(ln(n))\times m\times d \tag{9.3}$$

$\widehat{\Sigma}$ is $1/n$ times the residual sum of squares and cross-products matrix.

BIC promotes the most parsimonious model by putting the largest penalty on model complexity, followed by HQC and AIC. As such, we chose BIC as the default information criterion of DRMAT. By way of interpretation, the smaller the BIC, the more justified the balance of model fitting and model complexity. Whenever an additional breakpoint is added to the model, the top-down segmentation will demonstrate improved fitting as indicated by a continuous decrease in the residual sum of squares and cross-products matrix, but with an increase in the penalty component related to the number of parameters. The decision to add an additional breakpoint to the model depends on whether the current BIC is smaller than the previous one. The top-down segmentation stops when the BIC begins to rise, indicating that the model has reached its optimal balance of fitting and complexity.

Initial breakpoints were estimated based on the entire available multispectral time series, in which the trend and seasonality signal are coupled. This may increase the probability of ignoring a true breakpoint because the cost of adding an additional breakpoint is too high due to the coupling of trend and seasonality signals, thus the algorithm likely favors a lower number of breakpoints and hence leads to higher omission errors. However, we consider that breakpoints detected using the coupled signals have higher confidence because they are less likely to be added to the model unless the improvement of model fitting exceeds the penalty for model complexity. Therefore, we use them as an initial guess of the breakpoints for the following decomposition model, in this way, the algorithm efficiency will be improved.

2.2.2.2. Updating the breakpoints with the decomposed trend and seasonality signals. After getting initial breakpoints, DRMAT refines such segmentation of the multispectral time series with decomposed trend and seasonality signals as in Fig. 3:

i) Recording the initial breakpoints detected with undecomposed signals in list $\mathscr{L}$ (Fig. 3a). We also initialize the trend breakpoints $\mathscr{L}_T$ and seasonality breakpoints $\mathscr{L}_S$ to the breakpoints as in $\mathscr{L}$.
ii) Updating multivariate regression model with detected breakpoints. Specifically, if a multispectral time series $\boldsymbol{Y}_{n\times m}$ is divided into $(e+1)$ time segments by e breakpoints after the initial breakpoint detection, the design matrix $\boldsymbol{X_L}$ contains $8\times(e+1)$ columns: $2\times(e+1)$ trend columns and $6\times(e+1)$ seasonality columns; the parameter matrix $\boldsymbol{\beta_L}$ is a $(8\times(e+1))$ by m matrix, where m is the number of bands in the time series.
iii) De-seasonalizing the original multispectral time series using $\boldsymbol{Y}_{trend}+\boldsymbol{\varepsilon}=\boldsymbol{Y}-\widehat{\boldsymbol{Y}}_{season}$, where $\widehat{\boldsymbol{Y}}_{season}=\boldsymbol{X}_{\boldsymbol{L}(season)}\boldsymbol{\beta}_{\boldsymbol{L}(season)}$. In this case, $\boldsymbol{X}_{\boldsymbol{L}(season)}$ only contains the seasonality columns, which is an n by $6\times(e+1)$ matrix; the corresponding $\boldsymbol{\beta}_{\boldsymbol{L}(season)}$ only contains the parameters that determine the shape of seasonality signals, which is a $(6\times(e+1))$ by m matrix.
iv) Segmenting the multispectral time series based on the de-seasonalized time series $\boldsymbol{Y}_{trend}+\boldsymbol{\varepsilon}$. After getting trend breakpoints, we update $\mathscr{L}_T$ with newly detected p $(p=0,1,2\ldots)$ trend breakpoints and also update the multivariate regression model based on the current trend breakpoints. Note that now the trend breakpoints are differentiated from seasonality breakpoints, and hence the design matrix $\boldsymbol{X_L}$ will be updated. However, if no trend breakpoint is detected in the de-seasonalized signal, DRMAT will stop, unless this is the first attempt at detecting a trend breakpoint, as both sections of b and c in Fig. 3 should be performed at least once.
v) Detrending the original multispectral time series using $\boldsymbol{Y}_{season}+\boldsymbol{\varepsilon}=\boldsymbol{Y}-\widehat{\boldsymbol{Y}}_{trend}$, where $\widehat{\boldsymbol{Y}}_{trend}=\boldsymbol{X}_{\boldsymbol{L}(trend)}\boldsymbol{\beta}_{\boldsymbol{L}(trend)}$. Here, $\boldsymbol{X}_{\boldsymbol{L}(trend)}$ only contains the trend columns, which is a n by $2\times(p+1)$ matrix; the corresponding $\boldsymbol{\beta}_{\boldsymbol{L}(trend)}$ only contains the parameters that determine the shape of trend signals, which is a $(2\times(p+1))$ by m matrix.
vi) Segmenting the multispectral time series based on the detrended time series $\boldsymbol{Y}_{season}+\boldsymbol{\varepsilon}$. After getting seasonality breakpoints, we update $\mathscr{L}_S$ with newly detected q $(1=0,1,2\ldots)$ seasonality breakpoints and also update the multivariate regression model based on the current p trend and q seasonality breakpoints.
vii) Going back to step iii) until no more breakpoints in trend and seasonality are detected.

3. Evaluation

We quantitatively and qualitatively evaluated DRMAT based on four case studies. In Case Study 1, we used simulated data to quantitatively evaluate whether DRMAT can detect the prescribed breakpoints in both trend and seasonality signals. We used a simulated dataset because the visual interpretation of real-world seasonality breakpoints is highly subjective, while a simulated dataset allows us to prescribe a known "true" scenario. Once the efficacy was verified using simulated data, we then applied it to real-world cases. In Case Studies 2 and 3, we used real-world datasets, randomly sampled from the Global Forest Change map (Hansen et al., 2013) and MapBiomas (Souza Jr et al., 2020), respectively, to quantitatively evaluate DRMAT. The former was used to examine the capability of DRMAT in detecting forest disturbances and subsequent recovery, and the latter was used to detect disturbances in a broad set of land cover types. In Case Study 4, we focused on a specific geographic region in Berkeley-Oakland California, the United States. This region encountered various land disturbances from 1982 to 2018. We qualitatively evaluated DRMAT's effectiveness in mapping spatio-temporal patterns of disturbances in this region.

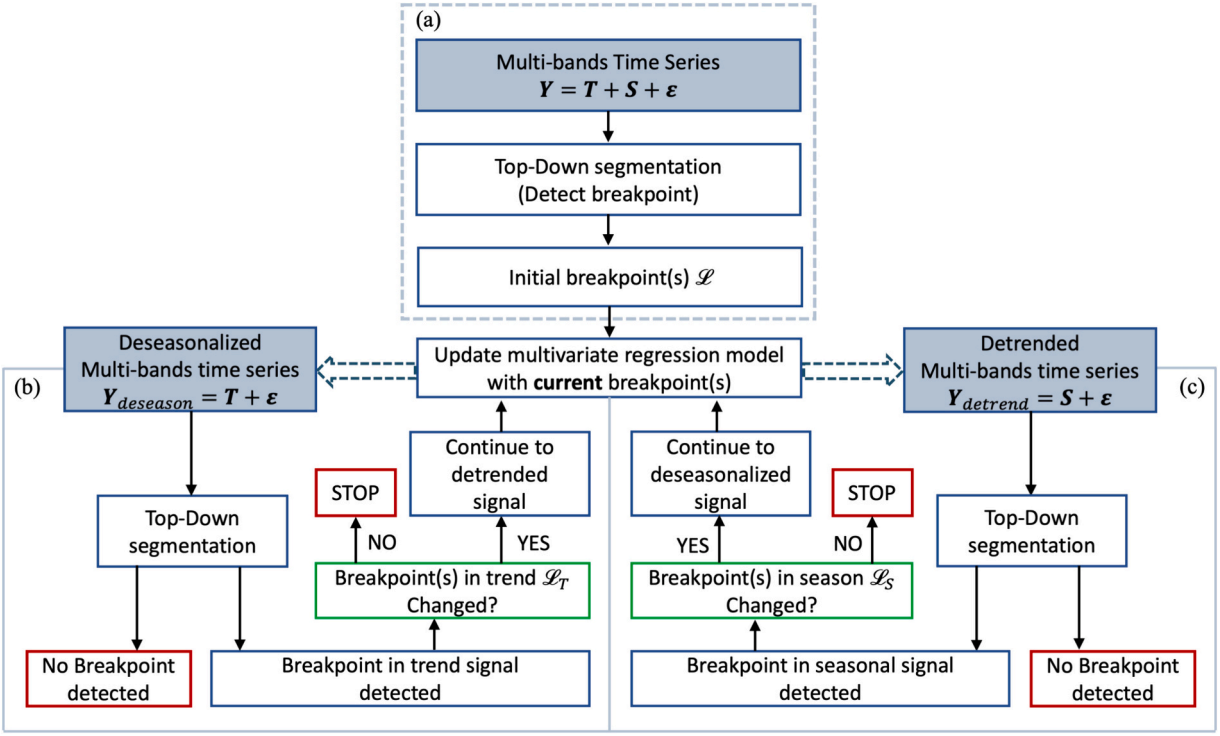

Fig. 3. The framework of DRMAT. The filled blue rectangle is the input data. The unfilled blue, green, and red rectangles are detection procedures, decision rules, and end nodes, respectively. The dashed arrow indicates that the deseasonality section (b) and detrend section (c) are not performed simultaneously but sequentially. DRMAT chooses one side each time and uses the output of one section (i.e., de-seasonalized signal of b or detrended signal of c) as the input of the other section. (For interpretation of the references to colour in this figure legend, the reader is referred to the web version of this article.)

3.1. Case study 1: simulated multispectral time series

Real-world time series are necessary for algorithm evaluation, but it is difficult to distinguish whether a breakpoint occurs in a trend signal or a seasonality signal through visual interpretation, and such limitation in reference data prevents a comprehensive evaluation of DRMAT using real-world time series. Moreover, real-world pixels that are perturbed multiple times over decades are uncommon (Hermosilla et al., 2019), challenging the evaluation of the algorithm using real-world time series. Compared to real-world time series, simulated multivariate time series provides a tractable way to assign multiple breakpoints in both trend and seasonality signals and to validate the results with prescribed breakpoints, therefore has been adopted in this study to evaluate the accuracy of DRMAT in detecting breakpoints.

The simulation data were generated as the sum of three components as we introduced in Section 2.2.1: trend, seasonality, and noise. Each simulated time series spanned 20 years with 0–3 breakpoints randomly sampled in trend and seasonality signals, respectively. Trend signals were considered as piecewise linear, with two coefficients (i.e., slope and intercept) randomly sampled from a multivariate Gaussian distribution. The seasonality signals were piecewise harmonics with three frequencies and thus six coefficients (i.e., three sines and three cosines), all of which were randomly sampled from another multivariate Gaussian distribution. Both Gaussian distributions were fitted from 200 real multivariate time series that would be introduced in Case Study 2 (Section 3.2). Therefore, this simulated dataset is more representative of disturbances in deciduous forests.

It is worth noting that trend/seasonality signals from different bands may not be correlated with each other, but noise signals from different bands are correlated with each other because of a couple of factors, such as the contamination by clouds or aerosols at the same time and location, the topography, and the overlap among sensor bands (Schowengerdt, 2006). Therefore, we adjusted the correlation of noise among bands by adjusting the off-diagonal elements in the residuals' correlation matrix, which was also generated from the 200 real multivariate time series.

To ensure that the signal variation at breakpoints in trend (seasonality) is not covered up by the signal variation of the seasonality (trend) and noise, we rescaled the variance of trend and seasonality signals to the same and simulated noise based on varying levels of 2 % ~ 20 % of data noise. Based on the abovementioned rules, a total number of 200 simulated time series were generated, with 416 breakpoints in the trend signal and 435 breakpoints in the seasonality signal; 13 out of 200 time series have no breakpoints in either trend or seasonality signal (Fig. S1).

3.2. Case study 2: Subtle land changes due to forest disturbances and recovery

3.2.1. Data sampling

To assess the accuracy of DRMAT in detecting forest disturbances and subsequent recovery, we sampled 200 sites in temperate deciduous forests in the United States. For each of these sites, we obtained Landsat multispectral surface reflectance time series spanning from 2001 to 2020, detected their breakpoints based on DRMAT, and compared them with a reference dataset. Here, breakpoints included both disturbances and subsequent recovery (White et al., 2017) because both could lead to signal shifts in trend or seasonality signals. The reference dataset was provided by examining remote sensing images at each site via TimeSync (Cohen et al., 2010) and Google Earth. For simplicity, we only sampled temperate deciduous forests in the United States that experienced disturbance in 2005 and recovered afterward using the procedure described below. Doing so allowed the detection of breakpoints caused by both disturbances and recovery. We also examined the site images from 2006 to 2020 to identify the years of recovery.

A two-step procedure was employed to ensure that the disturbance occurred in 2005 and that forests could be recovered. Firstly, the Global

Forest Change map (Hansen et al., 2013) was used to locate forest pixels in the temperate region in the United States that were only disturbed in 2005, with no forest loss in all other years. To reduce the possibility of sampling misclassified pixels in the Global Forest Change map, each pixel we sampled was the central pixel of a 3 × 3 image chip, where all pixels satisfied the abovementioned criterion to minimize the risk of sampling a misclassified pixel. Then, to exclude pixels classified as forest losses with no recovery, we overlaid all the pixels with the USGS National Land Cover Database, a set of land cover maps that include years of 2001, 2004, 2006, 2008, 2011, 2013, 2016, and 2019, and chose only those classified as "deciduous" in 2001 and 2004, "non-forest" in 2006, 2008, followed by the same forest type again in 2011, 2013, 2016, and 2019. After this two-step procedure, we sampled 200 pixels from all the candidates and extracted their multispectral surface reflectance from Landsat, including bands 1–7, which are blue, green, red, near-infrared (NIR), shortwave infrared 1 (SWIR1), shortwave infrared 2 (SWIR2) and surface temperature bands, respectively. All pixels were quality assessed. Detected breakpoints with decreasing Normalized Difference Vegetation Index (NDVI) would be classified as disturbances, while with increasing NDVI would be classified as recovery. Generally, disturbances refer to vegetation depletion and degradation (a negative signal), while recovery is considered as the return of vegetation following a disturbance (a positive signal). It's important to note that we are not making statements regarding metrics aimed at indicating the return of vegetation after a disturbance but rather using the multidirectional nature of the DRMAT to inform on the directionality of the change.

Based on the ground reference of the 200 sampled sites, a total number of 414 changepoints have been recorded via visual interpretation based on TimeSync and Google Earth, including 197 disturbances and 217 exhibiting recovery. For disturbances, though the sampling procedure focused on forest disturbances that occurred in 2005, some disturbances occurred in 2004 as visually detected in the TimeSync and Google Earth. The inconsistency between the disturbance year indicated by the Global Forest Change map and by visual interpretation was likely caused by the timing of disturbances because the derivation of the Global Forest Change map was based on growing season data. Hence, disturbances that occurred at the end of 2004 could be detected by visual interpretation in 2004 but could only captured by the Global Forest Change map in the following year. Therefore, the disturbance year from visual interpretation was used if the two results were inconsistent. Meanwhile, some sites with disturbances that occurred in years other than 2004 and 2005 have been sampled, we recorded their disturbed year based on visual interpretation in the reference data; three sites with two disturbances respectively have also been sampled, and we recorded both disturbances in each site in the reference data. Additionally, for 6 of the 200 sites, we did not observe any disturbances in TimeSync or Google Earth, so we did not record any disturbances in them. For recovery, we marked the year with a sign of greening as the recovery year. In some sites, a complete recovery (i.e., no difference compared to adjacent non-disturbed forests) also has been observed after the greening in some disturbed sites (Li et al., 2022b), we regarded it as a second recovery and recorded both recoveries in the reference data.

3.2.2. Baseline models

We conducted multiple tests and comparisons to evaluate the performance of DRMAT in detecting breakpoints in the real world, including both disturbances and recovery. We compared the DRMAT model with its corresponding univariate model— top-down segmentation, demonstrating the better performance of using multivariate methods (Section 4.2.2). We could also compare our multivariate model to other univariate models, such as the COntinuous monitoring of Land Disturbance (COLD) algorithm. However, COLD and DRMAT are totally different models, not only in their univariate/multivariate methodologies but also in their base algorithms. COLD is categorized as a statistical boundary method that expects the time series to follow a statistical boundary; any significant departure from the boundary is defined as a breakpoint (Zhu et al., 2020). In contrast, DRMAT is a multivariate segmentation method and the connection of two segments is defined as a breakpoint. Therefore, distinguishing the sources of difference in the results between the two models is challenging. The observed differences could arise from the distinct univariate/multivariate methodologies or from the varying effectiveness of the base algorithms in detecting breakpoints. Considering that our multivariate model is built upon the top-down segmentation, the univariate model we used for comparison also employs the segmentation algorithm as its base algorithm.

We also investigated whether increasing the input information would enhance the overall accuracy of our model (Section 4.2.3). To further evaluate the potential benefits of incorporating more information, we conducted experiments that used NDVI, NDMI, and NBR as additional input (Section 4.2.4) as additional model inputs. NDVI serves as a renowned indicator of vegetation status, while NDMI and NBR are widely used in the context of forests. Additionally, we compared DRMAT with the other two baselines, including DRMAT without differentiating breakpoints in trend and seasonality (Section 4.2.5), and DRMAT with different information criteria (Section 4.2.6).

3.3. Case study 3: subtle land changes in broader land cover types

To evaluate the accuracy of DRMAT in detecting subtle land changes in broader land cover types, we randomly sampled 200 sites from MapBiomas. MapBiomas provides annual land use and land cover information in Brazil, with five major classes in total (i.e., forests, non-forest natural formation, farming lands, non-vegetated areas, and water) (Souza et al., 2020). Each major class contains several sub-classifications, providing detailed insights into the landscape composition.

To examine the capability of DRMAT in detecting subtle land disturbances rather than only high-magnitude changes, we focused on pixels that changed among forests, non-forest natural formations, and farming lands, excluding pixels that were once marked as non-vegetated areas or water. Additionally, to ensure data quality, we excluded border pixels and pixels with a low level of agreement. The final randomly sampled 200 sites experienced land conversions across a range of land covers, including "Forest Plantation", "Forest Formation", "Savanna Formation", "Grassland", "Pasture", "Temporary Crop", "Perennial Crop", and "Wetland", with wetland only being observed in two sample sites.

For each sampled site, we accessed its Landsat multispectral time series from 1984 to 2020 through Google Earth Engine, with disturbances possibly occurring in any year within this timeframe (Fig. S2). Based on the provided coordinates for each sampled site, we used satellite images via TimeSync and Google Earth to confirm the presence of recorded land cover changes in the validation dataset. If a recorded change in a particular year was not observed in both satellite images, it was then classified as "no disturbance" in the reference dataset. However, if a significant change in a year was observed in both satellite images but was not initially recorded in the reference dataset, we added that year as a "disturbance" accordingly. In total, 200 time series with 407 breakpoints were sampled, with at least one disturbance occurring in each time series.

3.4. Case study 4: Disturbance map in Berkeley-Oakland

To assess the capability of DRMAT in capturing both the timing and the location of disturbances compared to conventional univariate approaches, we mapped disturbances in Berkeley-Oakland region in California, USA, ranging from 122°9′ W to 122°23′ W and from 37°47′ N to 37°54′ N (Fig. 4a). This region was adopted by COLD algorithm in their study to evaluate the model capability in detecting disturbances (Zhu et al., 2020). It has experienced multiple disturbances, such as Oakland Fire in 1991 (Fig. 4f), reconstruction of Interstate 80 in California during the 1990s (Fig. 4b), Port of Oakland development in early 2000s

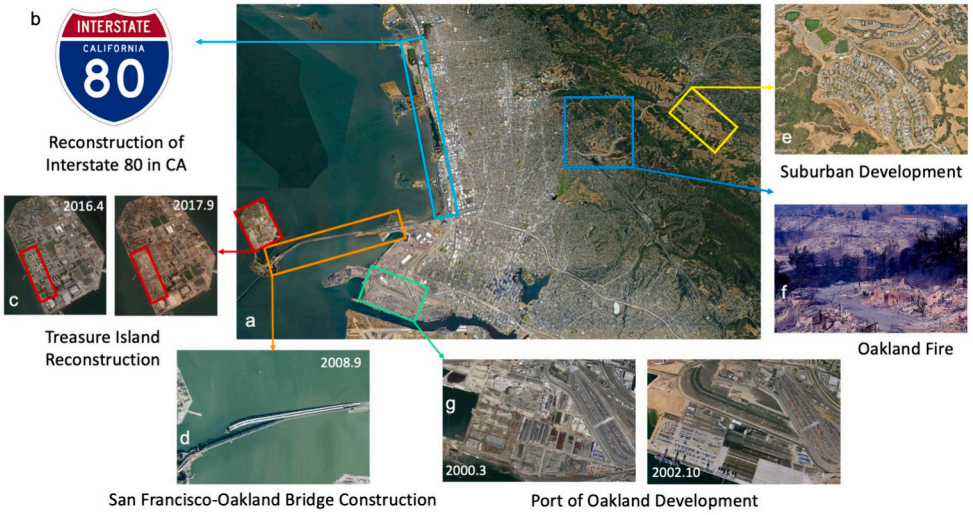

Fig. 4. Major land disturbances in the Berkeley-Oakland region from 1982 to 2018. (a) A satellite image for the Berkeley-Oakland region. (b) Reconstruction of Interstate 80 in California during the 1990s. (c) Treasure Island comparison between April 2016 and September 2017. (d) San Francisco-Oakland Bridge construction image in September 2008. (e) Suburban development in Wilder, Orinda, California. (f) Oakland Fire in 1991. (g) Port of Oakland comparison between March 2000 and October 2002. All images are from Google Earth except for the Oakland fire and Interstate 80 reconstruction, which are from Berkeley News (October 13, 2017) and Wikipedia of Interstate 80, respectively.

(Fig. 4g), Suburban development in Wilder, Orinda since 2007 (Fig. 4e), San Francisco-Oakland Bridge construction at the end of 2000s (Fig. 4d), and Treasure Island Reconstruction after mid-2010s (Fig. 4c). Considering that COLD's analysis covered the period from 1982 to February 15, 2018, we chose to evaluate DRMAT over the same timeframe to facilitate direct comparison of the results. Landsat surface reflectance data spanning from 1982 to February 15, 2018 were used in our study. We adopted AIC here to capture as much historical land disturbances as possible in the map.

3.5. Accuracy assessment

To assess the accuracy of the DRMAT algorithm, commission error, omission error, and the F1 score were calculated (Shang et al., 2022; Zhu et al., 2020). Commission error (i.e., false positive rate) measures the rate of breakpoints that are detected by the algorithm yet not labeled in the reference data. Omission error (i.e., false negative rate) measures the rate of breakpoints that exist in the reference data yet fail to be detected by the algorithm. Decreasing commission error by being parsimonious on the newly detected breakpoints will increase the omission error because breakpoints will tend to not be detected, and vice versa. Therefore, we also used the F1 score as a third metric to balance the commission error and omission error.

4. Results

4.1. Case study 1: quantitative evaluation using simulated multispectral time series

The validation of DRMAT was performed on the year level: as long as the year of the detected breakpoint is consistent with the year of the referenced breakpoint, we considered the detected result to be correct. Results showed that DRMAT unveiled breakpoints in both trend and seasonality signals, with a better performance in seasonality, supporting the efficacy of the algorithm in detecting the underlying breakpoints. Both commission error and omission error in seasonality were lower than 10 %, contributing to an F1 score of 91.7 %. For the breakpoints in trend, although the omission error was as low as 3.9 % (i.e., producer's accuracy of 96.1 %), the high commission error of 23.3 % (i.e., user's accuracy of 76.7 %) caused a relatively low F1 score of 85.5 %.

4.2. Case study 2: Quantitative evaluation using forest disturbances and recovery

4.2.1. The breakpoints detected by DRMAT

DRMAT was able to detect most of the changepoints in the reference dataset, though unavoidably with commission and omission errors. Overall, it performed better in detecting disturbances rather than recovery, with an omission error of 5.2 % (i.e., producer's accuracy as 94.8 %) and a commission error of 4.6 % (i.e., user's accuracy as 95.4 %). In contrast, the omission error for detected recovery increased to 36.4 % (i.e., producer's accuracy as 63.6 %) and the corresponding commission error slightly decreased to 2.1 % (i.e., user's accuracy as 97.9 %). So, the F1 scores of detected disturbances and recovery were 95.1 % and 77.1 %, respectively. The lower accuracy of recovery detection was expected because compared to abrupt changes in surface reflectance after disturbances, situations relating to recovery were gradual thus more challenging to identify. Such slower changes during the recovery process not only led to a higher omission error of breakpoint detection but also brought in larger uncertainty in visually detected recovery.

4.2.2. Multivariate approach vs. univariate approach

The multivariate approach outperforms the univariate approach in all three metrics: commission error, omission error, and F1 score, either for detected disturbances or recovery (Fig. 5). For disturbances, the multivariate approach detected 196 disturbances, whereas the univariate approach detected a higher count of 465 disturbances. However, considering that there were only 197 reference disturbances, the univariate approach exhibited a notably high commission error of 60 %. Consequently, the F1 score of the univariate approach (56.2 %) is much lower compared to the F1 score of the multivariate approach (95.1 %) for detected disturbances. For recovery, the univariate approach performed less effectively than the multivariate approach in both commission error and omission error, consequently leading to a lower F1 score of 34.7 % as compared to the F1 score of the multivariate approach (77.1 %).

4.2.3. Multispectral bands sensitivity analysis

To examine whether incorporating all-band information into the model gives the best result, we also detected disturbances and recovery

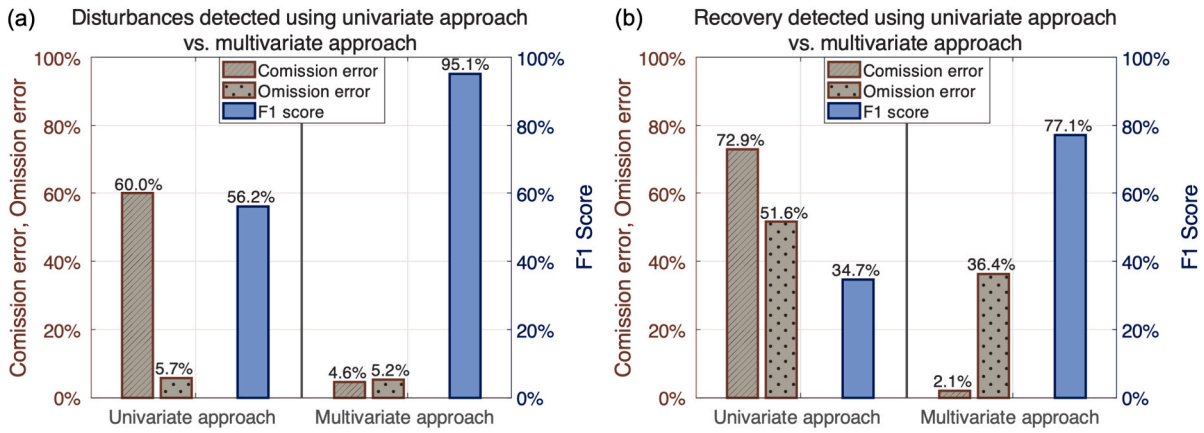

Fig. 5. Metrics of detected disturbances (a) and recovery (b) using univariate and multivariate approaches, respectively. Each subplot consists of two panels, with the left panel displaying metrics for the univariate approach and the right panel showing metrics for the multivariate approach. Error metrics are represented in grey colour, with the line bar indicating commission error and the dots bar representing omission error. The accuracy metrics, F1 score, is represented in blue bars. (For interpretation of the references to colour in this figure legend, the reader is referred to the web version of this article.)

using different combinations of bands. As input bands increased, the highest F1 score of detected disturbances and recovery increased, indicating that the accuracy of both detected disturbances and recovery improved, with detected disturbances showing higher accuracy than detected recovery. From one band to seven-band combinations, only 3 out of 120 combinations had F1 scores above 90 % for detected disturbances and above 70 % for detected recovery (Fig. 6). The seven-band combination gave the highest F1 scores (i.e., 95.1 % for disturbance and 77.1 % for recovery); followed by the five-band combination of Green, Red, NIR, SWIR1 and SWIR2, with F1 score of 93.3 % for disturbance and of 74.5 % for recovery (Fig. 6). A six-band combination of Green, Red, NIR, SWIR1, SWIR2, and ST showed a F1 score of 92.7 % for disturbance and of 73.1 % for recovery (Fig. 6).

4.2.4. The breakpoints detected by DRMAT with vegetation indices as additional inputs

To test if adding vegetation indices helped the breakpoints detection, we first took all seven bands as model input, then added different vegetation indices to see whether the overall accuracy improved. The red plane (red line) in Fig. 7 indicates where commission errors equal to 20 %. When seven bands were used as input, the overall accuracy was already high (i.e., points located on the left side of the red plane), adding NDVI, Normalized Difference Moisture Index (NDMI) and Normalized Burn Ratio (NBR) did not show much improvement as the positions of blue and orange points on the left side did not change much (Fig. 7). We then tested whether, given fewer bands as input, adding additional information from the vegetation index would help to improve the overall accuracy. We chose three bands (i.e., blue, green, and red) as a baseline, and the accuracy metrics from the three-bands were much worse than from seven-bands and lay on the right side of the red plane (Fig. 7). Adding NDVI increased the F1 scores of disturbances from 62.6 % to 67.8 %, and increased the F1 scores of recovery from 20.4 % to 41.1 %. We also used NDMI and NBR as additional inputs because they provided new information from shortwave near-infrared bands. Adding NDMI and NBR increased the F1 scores of disturbances to 79.7 % and 78.1 %, respectively; and increased the F1 scores of recovery to 54.4 % and 58.2

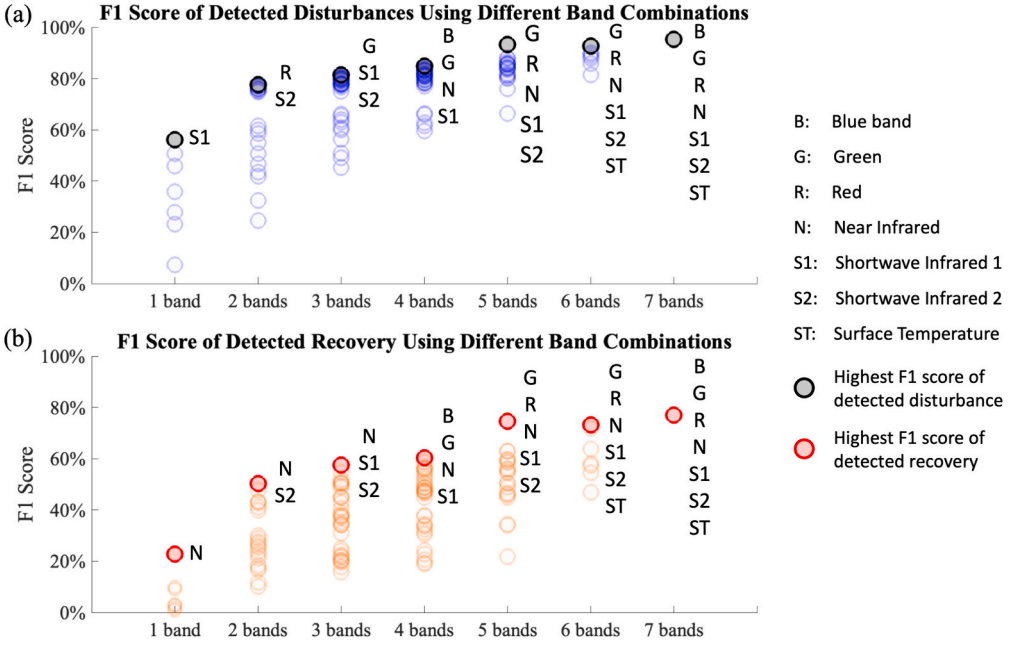

Fig. 6. F1 scores of detected breakpoints (i.e., disturbances and recovery) using different band combinations. The vertical labels indicate the band combinations with the best F1-score for each band group, showing an overall increase in detection accuracies with more input bands.

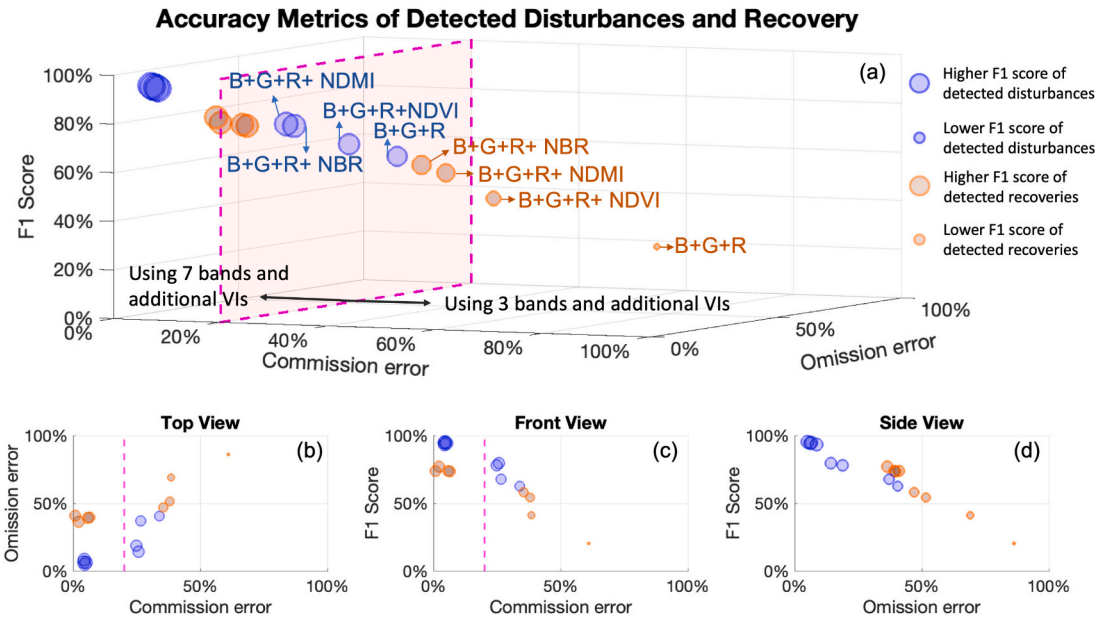

Fig. 7. The accuracy metrics of detected disturbance and recovery using different bands and additional vegetation index as inputs, with a three-dimensional view (a), a top view (b), a front view (c), and a side view (d). Red plane in (a) and red lines in (b) and (c) indicate where the commission error equals 20 %. Blue and orange points refer to the accuracy metrics of detected disturbances and recovery, respectively. The higher the F1 score, the larger the point size. B is the blue band, G is the green band, R is the red band, and VI indicates the vegetation index. (For interpretation of the references to colour in this figure legend, the reader is referred to the web version of this article.)

%, respectively.

4.2.5. *The breakpoints detected by DRMAT without differentiating trend and seasonality*

To test whether differentiating breakpoints in trend and seasonality improved the overall accuracy, we also detected breakpoints using DRMAT without differentiating trend and seasonality (DRMAT_w/o). Compared to the results detected by DRMAT, both commission error and omission error increased. Commission error increased from 4.6 % to 10.5 % for disturbances, and from 2.1 % to 16.3 % for recovery; omission error notably increased from 5.2 % to 82.7 % for disturbance and from 36.4 % to 81.1 % for recovery. Instead of using either detrended or de-seasonalized signals as inputs as DRMAT did (Fig. 3), DRMAT_w/o used the coupled signals. Therefore, whenever detecting a new breakpoint, the design matrix in DRMAT would be updated with either 6 columns (if it was a seasonality breakpoint) or 2 columns (if it was a trend breakpoint), but the design matrix in DRMAT_w/o would be updated with extra 8 columns, resulting in more penalty when deciding whether the new breakpoint should be added to the current model. As a result, fewer breakpoints would be kept in the model and thus omission errors increased. Results from this study supported the advantage of DRMAT in effectively detecting breakpoints in seasonality or trend separately.

4.2.6. *Information criteria sensitivity analysis*

In DRMAT, the most parsimonious version with BIC as an information criterion detected the fewest breakpoints (i.e., disturbances and recovery), followed by HQC and AIC (Table 1). The decrease in detected breakpoints, therefore, led to an increase in omission errors and a decrease in commission errors. From Table 1, BIC resulted in the least number of disturbances and recovery, leading to the highest omission errors and the lowest commission errors compared to the breakpoints detected using the other two information criteria. HQC, which put less penalty on an additional breakpoint, detected more disturbances and recovery compared to BIC, resulting in slightly lower omission errors but greatly higher commission errors, leading to lower F1 scores for both disturbances and recovery. AIC detected the most disturbances and recovery, resulting in omission errors of 0 % yet commission errors of more than 60 %, leading to the lowest F1 scores.

Table 1
Disturbance and recovery detection results based on different information criteria.

Criterion	Breakpoint type	Quantity	Commission error	Omission error	F1 score
AIC	Disturbance	557	64.6 %	0.0 %	52.3 %
	Recovery	675	67.9 %	0.0 %	48.7 %
HQC	Disturbance	262	25.6 %	1.0 %	85.0 %
	Recovery	301	35.2 %	10.1 %	75.3 %
BIC	Disturbance	196	4.6 %	5.2 %	95.1 %
	Recovery	141	2.1 %	36.4 %	77.1 %

4.3. *Case study 3: quantitative evaluation using subtle land changes in broader land cover types*

In the context of subtle land cover changes in broader land cover types, DRMAT detected most of the breakpoints in this examined dataset, with an omission error of 7.6 % (i.e., producer's accuracy as 92.4 %), a commission error of 23.0 % (i.e., user's accuracy as 77.0 %), and an F1 score of 84.0 %. However, compared to detecting forest disturbances, the overall performance of DRMAT in detecting subtle changes in broader land cover types is less effective. This is because the subtle land changes in Case Study 3 are less discernable than forest disturbances in Case Study 2. Notably, forest disturbances in Case Study 2 are typically caused by wildfire, thinning, or logging, thereby resulting in more pronounced differences in spectral bands before and after the disturbances. In contrast, detecting subtle land changes in Case Study 3 poses a significant challenge due to the inherent similarities between the involved land cover types, such as the land cover change from grassland

to pasture.

4.4. Case study 4: qualitative evaluation using disturbances map in Berkeley-Oakland

DRMAT captured the spatiotemporal patterns of disturbances demonstrated in Figure 4 in the Berkeley-Oakland region from 1982 to 2018. The accumulated disturbances detected by DRMAT from 1982 to 1991 revealed a few disturbed areas, with most disturbed pixels appearing to the right of the image center (Fig. 8a). These disturbed pixels overlapped with the reported area affected by the Oakland Fire in 1991 (Fig. 4f) (Zhu et al., 2020). The newly added disturbed pixels detected by DRMAT from 1992 to 1999 gathered along the coastal area, forming a line that traversed from north to south (Fig. 8b). These disturbed pixels showed the reconstruction of Interstate 80 in this area in the 1990s (Fig. 4b). The accumulated disturbances detected by DRMAT from 2000 to 2005 showed scattered development across the entire region, with a notable concentration in the lower left area of the land (Fig. 8c). This reflected the development of Port of Oakland in the early 2000s, as observed on Google Earth (Fig. 4g). After that, the right part of the image showed a clear disturbed area marked with yellow pixels, which can also be observed on Google Earth as the development of houses in Wilder, Orinda, starting approximately in 2007 (Fig. 8d, Fig. 4e). DRMAT continuously monitored this region until February 15, 2018, finding scattered disturbances across the entire region in the 2010s, but with more centered changes in the lower left corner of the image, such as the reconstruction on the Treasure Island (Fig. 8e, Fig. 4c).

The disturbance map derived from DRMAT (Fig. 8e) and COLD (Fig. 8f) show similarity in most areas, but DRMAT performs better in certain regions, notably in the white windows (Fig. 8g, h), where houses have been built up since 2007. Fig. 8i shows corresponding true-colour images. The areas "I" and "III" represent undisturbed areas and the area "II" represents the disturbed one. DRMAT accurately identified the disturbed area in "II" with a clearly delineated outline, whereas COLD detected disturbed pixels in all three areas, misidentifying undisturbed pixels in "I" and "III" as disturbed. However, the intention of this comparison is not to demonstrate the superiority of DRMAT over COLD, as COLD successfully detected the collapsed section of the Cypress viaduct of Interstate 880 resulting from the 1989 earthquake (Zhu et al., 2020), while DRMAT did not. Instead, our aim is to highlight this multivariate model, although built on top-down segmentation—a relatively rudimentary change detection method, demonstrates comparable performance to COLD—a pioneering model in the disturbance detection field.

5. Discussion

5.1. Comparison with previous models

Previous breakpoint detection models include various categories such as thresholding, differencing, segmentation, trajectory, statistical boundary, and regression (Zhu, 2017). To the best of our knowledge, all the reputable existing models in the remote sensing community follow an inherently univariate approach. This implies that they either apply

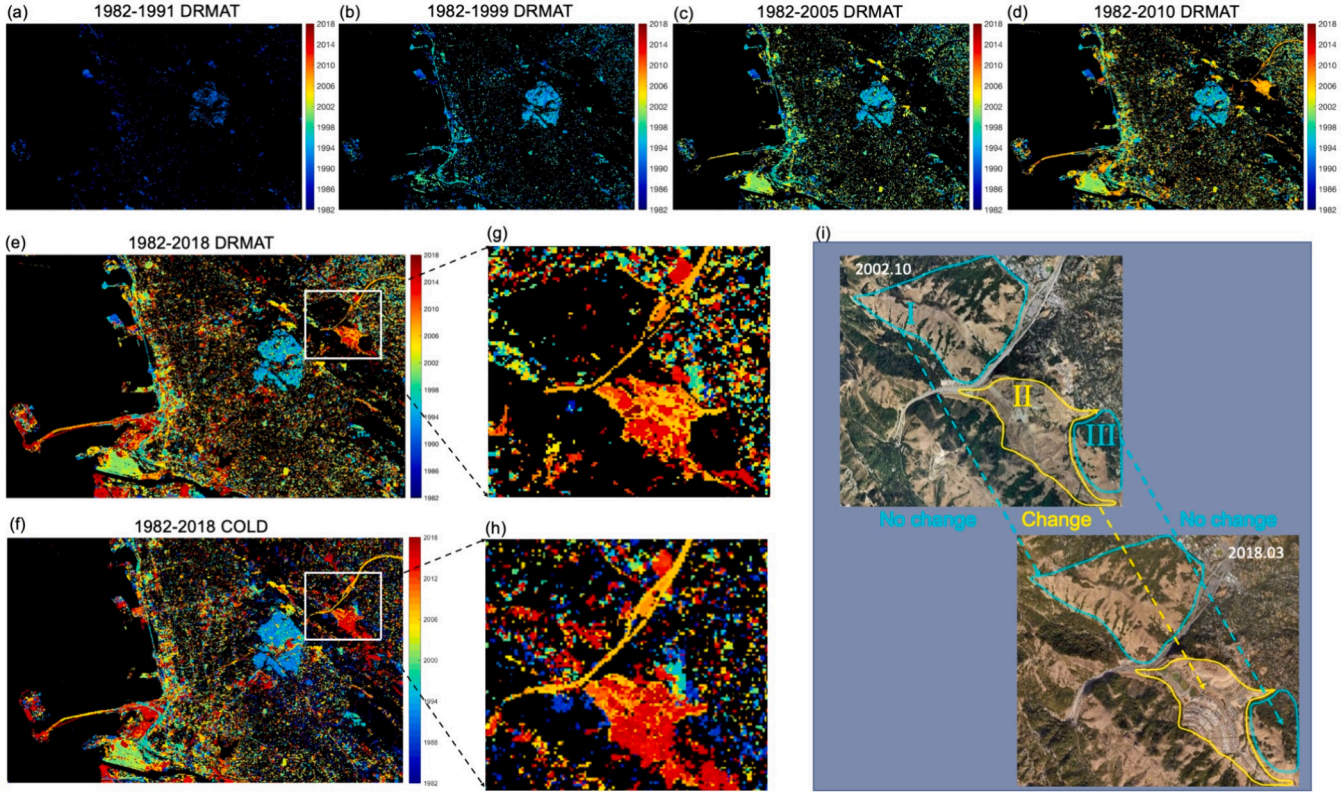

Fig. 8. Spatiotemporal patterns of disturbances detected by DRMAT and a univariate approach (i.e., COLD) over a selected region from 1982 to 2018. Cooler colors indicate disturbances occurring at earlier times, while warmer colors indicate disturbances occurring more recently. (a) to (e) are disturbances detected by DRMAT, while (f) is disturbances detected by COLD in the same region, as a comparison. (a) is accumulated disturbances detected by DRMAT from 1982 to 1991. (b) is accumulated disturbances detected by DRMAT from 1982 to 1999. (c) is accumulated disturbances detected by DRMAT from 1982 to 2005. (d) is accumulated disturbances detected by DRMAT from 1982 to 2010. (e) is accumulated disturbances detected by DRMAT from 1982 to 2018. (f) is accumulated disturbances detected by COLD from 1982 to 2018. (g) and (h) indicate zoomed-in views of the disturbances in the white windows in (e) and (f), respectively. (i) shows the land cover changes in the white window from October 2002 to March 2018, observed from Google Earth images. "I" and "III" represent the undisturbed areas that are marked by blue colour; whereas "II" represents the disturbed area that is marked by yellow colour. (For interpretation of the references to colour in this figure legend, the reader is referred to the web version of this article.)

models to individual bands or vegetation index and then integrate the results (Zhu et al., 2020; Zhu and Woodcock, 2014), or they adopt ensemble learning to combine various models, but the input for each model remains univariate (Cohen et al., 2020; Healey et al., 2018; Hu et al., 2024; Zhao et al., 2019). The development of DRMAT helps to bridge this gap by offering a multivariate approach that incorporates multispectral bands into time series analysis at the same time. Both quantitative and qualitative evaluations in this study demonstrated that DRMAT outperforms the univariate approach.

In addition, several well-known algorithms, such as LandTrendr, VCT, CCDC, and COLD algorithms, determine breakpoints by checking if some deviation metrics meet certain pre-set thresholds (Huang et al., 2010; Kennedy et al., 2010; Zhu et al., 2020; Zhu and Woodcock, 2014). Such methods either chose empirical change thresholds or relied heavily on threshold testing or criterion optimization. For instance, an empirical threshold of three times or Root Mean Square Error (RMSE) was adopted in CCDC (Zhu and Woodcock, 2014), which was then updated by Zhu et al. (2020) as a normalized change vector magnitude. However, such methods adopted a uniform threshold for all, yet true thresholds that could determine breakpoints may vary case by case. In contrast, DRMAT did not use pre-set thresholds, but determined breakpoints based on BIC, a widely used metric that was tailored for each time series. Similar approaches have also been adopted in models such as BFAST and BFAST Lite (Masiliūnas et al., 2021a, 2021b; Verbesselt et al., 2010a, 2010b), which helped to reduce the artificial bias caused by pre-set thresholds.

Compared to univariate approaches, multivariate approaches are not considered more computationally intensive but rather more efficient. For example, if a multi-spectral time series contains seven bands, univariate approaches need to run the model seven times and integrate the breakpoints derived from individual bands (Zhu et al., 2020; Zhu and Woodcock, 2014), while multivariate approaches only need to run the model once without integrating the results. Taking Case Study 3 as an example, it took 90.1 s (5 times average) for DRMAT to detect the breakpoints in all the 200 seven-band time series, whereas its corresponding univariate approach (i.e., top-down segmentation) took 138.3 s (5 times average) to conduct the same task. Currently, DRMAT is locally implemented in MATLAB, and the speed could be further improved if implemented in compiled programming languages such as C or C++.

5.2. The optimal band combination for breakpoint detection

Comparison of performance using different combinations of spectral bands supported the advantage of using all seven-bands, which yielded the highest F1 scores and was followed by a five-band combination of Green, Red, NIR, SWIR1, and SWIR2 (Fig. 6). The good performance of this five-band combination in breakpoints detection was also recognized by Zhu et al. (2020), especially in reducing the omission errors. However, increasing input bands from five selected bands to seven bands resulted in fewer detected breakpoints in both disturbances and recovery, leading to lower commission error and higher omission error. In the multivariate model, adding more bands as inputs led to more penalty in adding an additional breakpoint. Specifically, when only five bands were used as inputs, m in Eq. (9) equaled five; but when seven bands were used, m in Eq. (9) increased to seven, and hence the computed BIC would be increased, making it more difficult to add an additional breakpoint. Therefore, increasing the number of input bands from five to seven reduced the overall detected breakpoints and contributed to lower commission error and higher omission error. However, it is worth noting that omission error is usually taken more seriously than commission error as if a breakpoint is missed by the model, it will be missed forever; but if there are some false positives in the results, one can always reduce then by using some post-processing method. Therefore, taking the five bands or seven bands as input should be carefully discussed case by case.

A six-band combination of Green, Red, NIR, SWIR1, SWIR2, and ST also demonstrated high F1 scores in breakpoints detection, yet its F1 scores were still lower than the seven-band combination (Fig. 6). Although the exclusion of blue band was encouraged in previous studies because blue band was among the least important spectral regions for forest disturbance detection (Cohen et al., 2018), we demonstrated that incorporating blue band still decreased the commission error. Such improvement was possible due to the model structure of the multivariate algorithm.

Our study also highlights the importance of SWIR1 and SWIR2 bands in accurately detecting disturbances, as well as the effectiveness of the NIR band in detecting recovery. The sensitivity test indicates that SWIR1 and SWIR2 are consistently present in the band combinations that achieve the highest accuracy in identifying disturbances. Moreover, when the original input bands lack NIR and SWIR bands, the inclusion of NBR and NDMI, two vegetation indices that contain SWIR1 and SWIR2 bands, respectively, significantly improves the detection accuracy. This approach outperforms the use of NDVI, which lacks SWIR bands. Similarly, the NIR band is present in all the band combinations that achieve the highest accuracy in detecting recovery. The superior performance of SWIR bands in detecting disturbances is in line with previous studies by Cohen et al. (2018) and Schultz et al. (2016), and the performance of NIR band in detecting recovery is consistent with previous studies by Negrón-Juárez et al. (2020).

5.3. The trade-off between efficacy and accuracy

We used top-down segmentation to detect breakpoints in the decomposed trend and seasonality signals of a time series. The F1 score is higher than 85 % using simulation data, and higher than 77 % using real-world Landsat data, but optimization methods still exist. For example, once a breakpoint is determined by top-down segmentation, its location will not be changed, which gradually narrows down the possible combinations of breakpoints. However, previously determined breakpoints could still be optimized each time a new breakpoint is added to the model by, for example, adjusting the location of the previously determined breakpoints to test whether they can be substituted by nearby points. This optimization will increase the overall accuracy, but it is inevitably computationally expensive. Meanwhile, the Landsat time series used in this study is not an annual time series but with seasonal variations. Moving the breakpoint backward or forward may only update the perturbed month but does not contribute much to updating the detected perturbed year. Therefore, in this efficacy and accuracy trade-off, we chose top-down segmentation to capture the breakpoints with adequate accuracy and meanwhile to save computation time.

5.4. Limitation of the validation dataset

The quantitative and qualitative assessments of DRMAT were conducted on an annual basis because the availability of reference datasets on a monthly scale is limited, either images from TimeSync or from Google Earth. Meanwhile, when visually interpreting real-world disturbances, we found that visual interpretation of land disturbances was less reliable at the monthly level, with significant variability among independent observers, particularly in areas with subtle changes. Therefore, annual interpretation provides a more confident basis for validation datasets.

The necessity of validating change detection models on a specific time scale depends on their application scenarios. For instance, if a change detection model is used for continuous monitoring of the stock market, validation datasets may need to be at minute or even second scales. However, in the remote sensing field, where models are typically used for detecting land disturbances such as wildfires or insect infestations, large-scale wildfires can occur over months, while an insect infestation may span years (Mack et al., 2011; Nolè et al., 2022; Vogelmann et al., 2016; Ye et al., 2021). Thus, most existing change detection algorithms in the remote sensing field are validated on an annual scale (Huang et al., 2010; Hughes et al., 2017; Jin et al., 2013;

Zhao et al., 2019; Zhu et al., 2020; Zhu and Woodcock, 2014). With the advancements in remote sensing techniques and emerging scenarios demanding more precise disturbance detection, we anticipate that future efforts in disturbance detection models in the remote sensing field will prioritize enhancing both temporal and spatial resolution.

5.5. Science implications of DRMAT

The capability of DRMAT in detecting breakpoints in both trend and seasonality signals will benefit studies interested in subtle changes in vegetation; such changes could be in trend (e.g., post-disturbance recovery) or in seasonality (e.g., phenological shifts). Specifically, post-disturbance recovery of vegetation may be exhibited over different recovery stages, which are accompanied by different trends (Bartels et al., 2016; Kuuluvainen and Gauthier, 2018; Nguyen et al., 2018). Accurately detecting such trend shifts helps to determine the recovery stages and further helps to quantify the related energy and carbon balance. Besides, vegetation is also experiencing seasonality shifts in response to climate change, such shifts could be an advanced or delayed phenology (Meng et al., 2020; Piao et al., 2019; Wang et al., 2022b), or vegetation demographic changes (Felton et al., 2021; Heijmans et al., 2022). These reported seasonality shifts also impact the biophysical and biogeochemical processes and hence impact energy redistribution and carbon uptake and partitioning (Chen et al., 2022; Keenan et al., 2014). DRMAT can leverage the increasing availability of multisource satellite time-series data to detect such subtle seasonality shifts.

6. Conclusion

Compared to existing algorithms in the field, DRMAT is a true multivariate statistical method: it fully incorporated inter-correlation among bands, jointly estimated parameters, and avoided the need for integrating final results. DRMAT can decompose multivariate time series into trend, seasonality, and noise signals; reconstruct each branch signal and build a complete multivariate time series together; and most importantly, identify ecosystem dynamics and disturbances over time. Using both simulated data and real-world disturbances in forests and in broader land cover types, we demonstrated the potential of DRMAT in detecting breakpoints in multispectral time series. For simulation data, DRMAT detected prescribed breakpoints in both trend and seasonality signals with F1 scores higher than 85 %. For real-world data, DRMAT detected breakpoints caused by forest disturbances and following recovery with F1 scores of 95.1 % and 77.1 %, respectively. It also detected disturbances in broader land cover types with an F1 score of 84.0 %. The overall accuracy decreased if fewer bands were used as inputs. Our results indicated that DRMAT, as a multivariate model, outperforms the univariate approach significantly. We envision its eligibility in not only remote sensing data, but also in environmental, ecological, and socioeconomic time series data.

CRediT authorship contribution statement

Yang Li: Conceptualization, Methodology, Investigation, Software, Visualization, Formal analysis, Writing- original draft, Writing- review & editing, Data curation. **Michael A. Wulder:** Formal analysis, Methodology, Writing – review & editing. **Zhe Zhu:** Formal analysis, Methodology, Writing – review & editing. **Jan Verbesselt:** Formal analysis, Methodology, Writing – review & editing. **Dainius Masiliūnas:** Formal analysis, Methodology, Writing – review & editing. **Yanlan Liu:** Conceptualization, Data curation, Formal analysis, Investigation, Methodology, Writing – original draft, Writing – review & editing. **Gil Bohrer:** Methodology, Writing – review & editing. **Yongyang Cai:** Methodology, Writing – review & editing. **Yuyu Zhou:** Methodology, Writing – review & editing. **Zhaowei Ding:** Writing – review & editing. **Kaiguang Zhao:** Conceptualization, Formal analysis, Funding acquisition, Investigation, Methodology, Supervision, Writing – review & editing.

Declaration of competing interest

The authors declare that they have no known competing financial interests or personal relationships that could have appeared to influence the work reported in this paper.

Data availability

Data will be made available on request.

Acknowledgment

This work has been supported by the NASA Equity and Environmental Justice program (#21-EEJ21-0011), the USDA-NIFA (#2018–68002–27932), the Ohio Department of Higher Education (a Harmful Algal Bloom Research Initiative grant), the OARDC-SEED program (2016075), the Microsoft Azure for Research (CRM0518513), the University of Hong Kong HKU-100 Scholars Fund, and the USGS-NASA Landsat Science Team (LST) Program (140G0119C0008). We also thank Dr. Marie Weiss and all the anonymous reviewers for their constructive comments and suggestions.

Appendix A. Supplementary data

Supplementary data to this article can be found online at https://doi.org/10.1016/j.rse.2024.114402.

References

Adams, B.T., Matthews, S.N., Iverson, L.R., Prasad, A.M., Peters, M.P., Zhao, K., 2021. Spring phenological variability promoted by topography and vegetation assembly processes in a temperate forest landscape. Agricultural and Forest Meteorology 308, 108578.

Anderson, T.W., 1958. An Introduction to Multivariate Statistical Analysis, vol. 2. Wiley, New York, pp. 3–5.

Audibert, J., Michiardi, P., Guyard, F., Marti, S., Zuluaga, M.A., 2020. Usad: unsupervised anomaly detection on multivariate time series. In: Proceedings of the 26th ACM SIGKDD International Conference on Knowledge Discovery & Data Mining, pp. 3395–3404.

Bartels, S.F., Chen, H.Y., Wulder, M.A., White, J.C., 2016. Trends in post-disturbance recovery rates of Canada's forests following wildfire and harvest. For. Ecol. Manag. 361, 194–207.

Brewer, M.J., Butler, A., Cooksley, S.L., 2016. The relative performance of AIC, AICC and BIC in the presence of unobserved heterogeneity. Methods Ecol. Evol. 7 (6), 679–692.

Bright, R.M., Davin, E., O'Halloran, T., Pongratz, J., Zhao, K., Cescatti, A., 2017. Local temperature response to land cover and management change driven by non-radiative processes. Nat. Clim. Chang. 7 (4), 296–302.

Brooks, E.B., Thomas, V.A., Wynne, R.H., Coulston, J.W., 2012. Fitting the multitemporal curve: A Fourier series approach to the missing data problem in remote sensing analysis. IEEE Trans. Geosci. Remote Sens. 50 (9), 3340–3353.

Brooks, E.B., Wynne, R.H., Thomas, V.A., Blinn, C.E., Coulston, J.W., 2014. On-the-fly massively multitemporal change detection using statistical quality control charts and Landsat data. IEEE Trans. Geosci. Remote Sens. 52 (6), 3316–3332.

Brooks, E.B., Yang, Z., Thomas, V.A., Wynne, R.H., 2017. Edyn: dynamic signaling of changes to forests using exponentially weighted moving average charts. Forests 8 (9), 304.

Chance, C.M., Hermosilla, T., Coops, N.C., Wulder, M.A., White, J.C., 2016. Effect of topographic correction on forest change detection using spectral trend analysis of Landsat pixel-based composites. Int. J. Appl. Earth Obs. Geoinf. 44, 186–194.

Chen, C., Riley, W.J., Prentice, I.C., Keenan, T.F., 2022. CO2 fertilization of terrestrial photosynthesis inferred from site to global scales. Proc. Natl. Acad. Sci. 119 (10), e2115627119.

Chin, W., Cheah, J.H., Liu, Y., Ting, H., Lim, X.J., Cham, T.H., 2020. Demystifying the Role of Causal-Predictive Modeling Using Partial Least Squares Structural Equation Modeling in Information Systems Research. Industrial Management & Data Systems.

Cleveland, R.B., Cleveland, W.S., McRae, J.E., Terpenning, I., 1990. STL: A seasonal-trend decomposition. J. Off. Stat. 6 (1), 3–73.

Cohen, W.B., Yang, Z., Kennedy, R., 2010. Detecting trends in forest disturbance and recovery using yearly Landsat time series: 2. TimeSync—Tools for calibration and validation. Remote Sens. Environ. 114 (12), 2911–2924.

Cohen, W.B., Healey, S.P., Yang, Z., Stehman, S.V., Brewer, C.K., Brooks, E.B., Gorelick, N., Huang, C., Hughes, M.J., Kennedy, R.E., Loveland, T.R., 2017. How similar are forest disturbance maps derived from different Landsat time series algorithms? Forests 8 (4), 98.

Cohen, W.B., Yang, Z., Healey, S.P., Kennedy, R.E., Gorelick, N., 2018. A LandTrendr multispectral ensemble for forest disturbance detection. Remote Sens. Environ. 205, 131–140.
Cohen, W.B., Healey, S.P., Yang, Z., Zhu, Z., Gorelick, N., 2020. Diversity of algorithm and spectral band inputs improves Landsat monitoring of forest disturbance. Remote Sens. 12 (10), 1673.
Coppin, P., Jonckheere, I., Nackaerts, K., Muys, B., Lambin, E., 2004. Review ArticleDigital change detection methods in ecosystem monitoring: a review. Int. J. Remote Sens. 25 (9), 1565–1596.
Dashti, H., Chen, M., Smith, W.K., Zhao, K., Moore, D.J., 2024. Ecosystems Disturbance Recovery: What It Was or What It Could Have Been? Geophysical Research Letters 51 (17), e2024GL109219.
Davies, G.M., Vandvik, V., Marrs, R., Velle, L.G., 2022. Fire management in heather-dominated heaths and moorlands of North-West Europe. Global Appl. Prescrib. Fire 194.
Farwell, L.S., Gudex-Cross, D., Anise, I.E., Bosch, M.J., Olah, A.M., Radeloff, V.C., Razenkova, E., Rogova, N., Silveira, E.M., Smith, M.M., Pidgeon, A.M., 2021. Satellite image texture captures vegetation heterogeneity and explains patterns of bird richness. Remote Sens. Environ. 253, 112175.
Felton, A.J., Knapp, A.K., Smith, M.D., 2021. Precipitation–productivity relationships and the duration of precipitation anomalies: an underappreciated dimension of climate change. Glob. Chang. Biol. 27 (6), 1127–1140.
Fernandes, P.M., Davies, G.M., Ascoli, D., Fernández, C., Moreira, F., Rigolot, E., Stoof, C. R., Vega, J.A., Molina, D., 2013. Prescribed burning in southern Europe: developing fire management in a dynamic landscape. Front. Ecol. Environ. 11 (s1) e4-e14.
Frazier, R.J., Coops, N.C., Wulder, M.A., 2015. Boreal shield forest disturbance and recovery trends using Landsat time series. Remote Sens. Environ. 170, 317–327.
Gao, J., Meng, B., Liang, T., Feng, Q., Ge, J., Yin, J., Wu, C., Cui, X., Hou, M., Liu, J., Xie, H., 2019. Modeling alpine grassland forage phosphorus based on hyperspectral remote sensing and a multi-factor machine learning algorithm in the east of Tibetan plateau, China. ISPRS J. Photogramm. Remote Sens. 147, 104–117.
Gao, S., Zhong, R., Yan, K., Ma, X., Chen, X., Pu, J., Gao, S., Qi, J., Yin, G., Myneni, R.B., 2023. Evaluating the saturation effect of vegetation indices in forests using 3D radiative transfer simulations and satellite observations. Remote Sensing of Environment 295, 113665.
Gough, C.M., Bohrer, G., Hardiman, B.S., Nave, L.E., Vogel, C.S., Atkins, J.W., Bond-Lamberty, B., Fahey, R.T., Fotis, A.T., Grigri, M.S., Haber, L.T., 2021. Disturbance-accelerated succession increases the production of a temperate forest. Ecol. Appl. 31 (7), e02417.
Hamunyela, E., Verbesselt, J., Herold, M., 2016. Using spatial context to improve early detection of deforestation from Landsat time series. Remote Sens. Environ. 172, 126–138.
Hansen, M.C., Potapov, P.V., Moore, R., Hancher, M., Turubanova, S.A., Tyukavina, A., Thau, D., Stehman, S.V., Goetz, S.J., Loveland, T.R., Kommareddy, A., 2013. High-resolution global maps of 21st-century forest cover change. science 342 (6160), 850–853.
Hayes, D.J., Sader, S.A., 2001. Comparison of change-detection techniques for monitoring tropical forest clearing and vegetation regrowth in a time series. Photogramm. Eng. Remote. Sens. 67 (9), 1067–1075.
Healey, S.P., Cohen, W.B., Yang, Z., Brewer, C.K., Brooks, E.B., Gorelick, N., Hernandez, A.J., Huang, C., Hughes, M.J., Kennedy, R.E., Loveland, T.R., 2018. Mapping forest change using stacked generalization: an ensemble approach. Remote Sens. Environ. 204, 717–728.
Heijmans, M.M., Magnússon, R.Í., Lara, M.J., Frost, G.V., Myers-Smith, I.H., van Huissteden, J., Jorgenson, M.T., Fedorov, A.N., Epstein, H.E., Lawrence, D.M., Limpens, J., 2022. Tundra vegetation change and impacts on permafrost. Nat. Rev. Earth Environ. 3 (1), 68–84.
Hemati, M., Hasanlou, M., Mahdianpari, M., Mohammadimanesh, F., 2021. A systematic review of landsat data for change detection applications: 50 years of monitoring the earth. Remote Sens. 13 (15), 2869.
Hermosilla, T., Wulder, M.A., White, J.C., Coops, N.C., Hobart, G.W., 2015. An integrated Landsat time series protocol for change detection and generation of annual gap-free surface reflectance composites. Remote Sens. Environ. 158, 220–234.
Hermosilla, T., Wulder, M.A., White, J.C., Coops, N.C., 2019. Prevalence of multiple forest disturbances and impact on vegetation regrowth from interannual Landsat time series (1985–2015). Remote Sens. Environ. 233, 111403.
Hermosilla, T., Wulder, M.A., White, J.C., Coops, N.C., Hobart, G.W., Campbell, L.B., 2016. Mass data processing of time series Landsat imagery: pixels to data products for forest monitoring. International Journal of Digital Earth 9 (11), 1035–1054.
Hu, T., Toman, E.M., Chen, G., Shao, G., Zhou, Y., Li, Y., Zhao, K., Feng, Y., 2021. Mapping fine-scale human disturbances in a working landscape with Landsat time series on Google earth engine. ISPRS J. Photogramm. Remote Sens. 176, 250–261.
Hu, T., Zhang, X., Khanal, S., Wilson, R., Leng, G., Toman, E.M., Wang, X., Li, Y., Zhao, K., 2024. Climate change impacts on crop yields: A review of empirical findings, statistical crop models, and machine learning methods. Environmental Modelling & Software 106119.
Huang, C., Goward, S.N., Masek, J.G., Thomas, N., Zhu, Z., Vogelmann, J.E., 2010. An automated approach for reconstructing recent forest disturbance history using dense Landsat time series stacks. Remote Sens. Environ. 114 (1), 183–198.
Hughes, M.J., Kaylor, S.D., Hayes, D.J., 2017. Patch-based forest change detection from Landsat time series. Forests 8 (5), 166.
Jamali, S., Jönsson, P., Eklundh, L., Ardö, J., Seaquist, J., 2015. Detecting changes in vegetation trends using time series segmentation. Remote Sens. Environ. 156, 182–195.
Jin, N., Zeng, Y., Yan, K., Ji, Z., 2021. Multivariate air quality forecasting with nested long short term memory neural network. IEEE Trans. Industr. Inform. 17 (12), 8514–8522.
Jin, S., Yang, L., Danielson, P., Homer, C., Fry, J., Xian, G., 2013. A comprehensive change detection method for updating the National Land Cover Database to circa 2011. Remote Sens. Environ. 132, 159–175.
Kaptué, A.T., Prihodko, L., Hanan, N.P., 2015. On regreening and degradation in Sahelian watersheds. Proc. Natl. Acad. Sci. 112 (39), 12133–12138.
Keenan, T.F., Gray, J., Friedl, M.A., Toomey, M., Bohrer, G., Hollinger, D.Y., Munger, J. W., O'Keefe, J., Schmid, H.P., Wing, I.S., Yang, B., 2014. Net carbon uptake has increased through warming-induced changes in temperate forest phenology. Nat. Clim. Chang. 4 (7), 598–604.
Kennedy, R.E., Yang, Z., Cohen, W.B., 2010. Detecting trends in forest disturbance and recovery using yearly Landsat time series: 1. LandTrendr—temporal segmentation algorithms. Remote Sens. Environ. 114 (12), 2897–2910.
Kennedy, R.E., Andréfouët, S., Cohen, W.B., Gómez, C., Griffiths, P., Hais, M., Healey, S. P., Helmer, E.H., Hostert, P., Lyons, M.B., Meigs, G.W., 2014. Bringing an ecological view of change to Landsat-based remote sensing. Front. Ecol. Environ. 12 (6), 339–346.
Keogh, E., Chu, S., Hart, D., Pazzani, M., 2004. Segmenting time series: A survey and novel approach. In: Data Mining in Time Series Databases, pp. 1–21.
Kuuluvainen, T., Gauthier, S., 2018. Young and old forest in the boreal: critical stages of ecosystem dynamics and management under global change. Forest Ecosyst. 5 (1), 1–15.
Lawler, J.J., Lewis, D.J., Nelson, E., Plantinga, A.J., Polasky, S., Withey, J.C., Helmers, D. P., Martinuzzi, S., Pennington, D., Radeloff, V.C., 2014. Projected land-use change impacts on ecosystem services in the United States. Proc. Natl. Acad. Sci. 111 (20), 7492–7497.
Li, J., Roy, D.P., 2017. A global analysis of sentinel-2A, sentinel-2B and Landsat-8 data revisit intervals and implications for terrestrial monitoring. Remote Sens. 9 (9), 902.
Li, J., Li, Z.L., Wu, H., You, N., 2022a. Trend, seasonality, and abrupt change detection method for land surface temperature time-series analysis: Evaluation and improvement. Remote Sens. Environ. 280, 113222.
Li, Y., Liu, Y., Bohrer, G., Cai, Y., Wilson, A., Hu, T., Wang, Z., Zhao, K., 2022b. Impacts of forest loss on local climate across the conterminous United States: evidence from satellite time-series observations. Sci. Total Environ. 802, 149651.
Liu, D., Toman, E., Fuller, Z., Chen, G., Londo, A., Zhang, X., Zhao, K., 2018. Integration of historical map and aerial imagery to characterize long-term land-use change and landscape dynamics: an object-based analysis via random forests. Ecol. Indic. 95, 595–605.
Liu, L., Zhang, X., 2020. Effects of temperature variability and extremes on spring phenology across the contiguous United States from 1982 to 2016. Sci. Rep. 10 (1), 1–14.
Lu, D., Mausel, P., Brondizio, E., Moran, E., 2004. Change detection techniques. Int. J. Remote Sens. 25 (12), 2365–2401.
Ma, Q., Huang, J.G., Hänninen, H., Berninger, F., 2019. Divergent trends in the risk of spring frost damage to trees in Europe with recent warming. Glob. Chang. Biol. 25 (1), 351–360.
Mack, M.C., Bret-Harte, M.S., Hollingsworth, T.N., Jandt, R.R., Schuur, E.A., Shaver, G. R., Verbyla, D.L., 2011. Carbon loss from an unprecedented Arctic tundra wildfire. Nature 475 (7357), 489–492.
Masiliūnas, D., Tsendbazar, N.E., Herold, M., Lesiv, M., Buchhorn, M., Verbesselt, J., 2021a. Global land characterisation using land cover fractions at 100 m resolution. Remote Sens. Environ. 259, 112409.
Masiliūnas, D., Tsendbazar, N.E., Herold, M., Verbesselt, J., 2021b. Bfast lite: a lightweight break detection method for time series analysis. Remote Sens. 13 (16), 3308.
Meng, L., Mao, J., Zhou, Y., Richardson, A.D., Lee, X., Thornton, P.E., Ricciuto, D.M., Li, X., Dai, Y., Shi, X., Jia, G., 2020. Urban warming advances spring phenology but reduces the response of phenology to temperature in the conterminous United States. Proc. Natl. Acad. Sci. 117 (8), 4228–4233.
Mildrexler, D.J., Zhao, M., Heinsch, F.A., Running, S.W., 2007. A new satellite-based methodology for continental-scale disturbance detection. Ecol. Appl. 17 (1), 235–250.
Molenaar, P., Huizenga, H.M., Nesselroade, J.R., 2003. The relationship between the structure of interindividual and intraindividual variability: a theoretical and empirical vindication of developmental systems theory. In: Understanding Human Development, pp. 339–360.
Negrón-Juárez, R.I., Holm, J.A., Faybishenko, B., Magnabosco-Marra, D., Fisher, R.A., Shuman, J.K., de Araujo, A.C., Riley, W.J., Chambers, J.Q., 2020. Landsat near-infrared (NIR) band and ELM-FATES sensitivity to forest disturbances and regrowth in the Central Amazon. Biogeosciences 17 (23), 6185–6205.
Nguyen, T.H., Jones, S.D., Soto-Berelov, M., Haywood, A., Hislop, S., 2018. A spatial and temporal analysis of forest dynamics using Landsat time-series. Remote Sens. Environ. 217, 461–475.
Nickerson, S., Chen, G., Fearnside, P.M., Allan, C.J., Hu, T., de Carvalho, Zhao, K., 2022. Forest loss is significantly higher near clustered small dams than single large dams per megawatt of hydroelectricity installed in the Brazilian Amazon. Environmental Research Letters 17 (8), 084026.
Nolè, A., Rita, A., Spatola, M.F., Borghetti, M., 2022. Biogeographic variability in wildfire severity and post-fire vegetation recovery across the European forests via remote sensing-derived spectral metrics. Sci. Total Environ. 823, 153807.
Piao, S., Liu, Q., Chen, A., Janssens, I.A., Fu, Y., Dai, J., Liu, L., Lian, X.U., Shen, M., Zhu, X., 2019. Plant phenology and global climate change: current progresses and challenges. Glob. Chang. Biol. 25 (6), 1922–1940.

Potapov, P.V., Turubanova, S.A., Tyukavina, A., Krylov, A.M., McCarty, J.L., Radeloff, V. C., Hansen, M.C., 2015. Eastern Europe's forest cover dynamics from 1985 to 2012 quantified from the full Landsat archive. Remote Sens. Environ. 159, 28–43.
Quesada, B., Arneth, A., Robertson, E., de Noblet-Ducoudré, N., 2018. Potential strong contribution of future anthropogenic land-use and land-cover change to the terrestrial carbon cycle. Environ. Res. Lett. 13 (6), 064023.
Rhif, M., Abbes, A.B., Martinez, B., de Jong, R., Sang, Y., Farah, I.R., 2022. Detection of trend and seasonal changes in non-stationary remote sensing data: case study of Tunisia vegetation dynamics. Eco. Inform. 69, 101596.
Schowengerdt, R.A., 2006. Remote Sensing: Models and Methods for Image Processing. Elsevier.
Schroeder, T.A., Schleeweis, K.G., Moisen, G.G., Toney, C., Cohen, W.B., Freeman, E.A., Yang, Z., Huang, C., 2017. Testing a Landsat-based approach for mapping disturbance causality in US forests. Remote Sens. Environ. 195, 230–243.
Schultz, M., Clevers, J.G., Carter, S., Verbesselt, J., Avitabile, V., Quang, H.V., Herold, M., 2016. Performance of vegetation indices from Landsat time series in deforestation monitoring. Int. J. Appl. Earth Obs. Geoinf. 52, 318–327.
Seidl, R., Thom, D., Kautz, M., Martin-Benito, D., Peltoniemi, M., Vacchiano, G., Wild, J., Ascoli, D., Petr, M., Honkaniemi, J., Lexer, M.J., 2017. Forest disturbances under climate change. Nat. Clim. Chang. 7 (6), 395–402.
Shang, R., Zhu, Z., Zhang, J., Qiu, S., Yang, Z., Li, T., Yang, X., 2022. Near-real-time monitoring of land disturbance with harmonized Landsats 7–8 and Sentinel-2 data. Remote Sens. Environ. 278, 113073.
Singh, A., 1989. Review article digital change detection techniques using remotely-sensed data. Int. J. Remote Sens. 10 (6), 989–1003.
Souza Jr., C.M., Shimbo, Z., Rosa, M.R., Parente, L.L., Alencar, A., Rudorff, B.F., Hasenack, H., Matsumoto, M., Ferreira, L., Souza-Filho, P.W., De Oliveira, S.W., 2020. Reconstructing three decades of land use and land cover changes in brazilian biomes with landsat archive and earth engine. Remote Sens. 12 (17), 2735.
Stergiou, K.I., Christou, E.D., 1996. Modelling and forecasting annual fisheries catches: comparison of regression, univariate and multivariate time series methods. Fish. Res. 25 (2), 105–138.
Swartz, M.D., Yu, R.K., Shete, S., 2008. Finding factors influencing risk: comparing Bayesian stochastic search and standard variable selection methods applied to logistic regression models of cases and controls. Stat. Med. 27 (29), 6158–6174.
Tewkesbury, A.P., Comber, A.J., Tate, N.J., Lamb, A., Fisher, P.F., 2015. A critical synthesis of remotely sensed optical image change detection techniques. Remote Sens. Environ. 160, 1–14.
Verbesselt, J., Hyndman, R., Newnham, G., Culvenor, D., 2010a. Detecting trend and seasonal changes in satellite image time series. Remote Sens. Environ. 114 (1), 106–115.
Verbesselt, J., Hyndman, R., Zeileis, A., Culvenor, D., 2010b. Phenological change detection while accounting for abrupt and gradual trends in satellite image time series. Remote Sens. Environ. 114 (12), 2970–2980.
Vogelmann, J.E., Gallant, A.L., Shi, H., Zhu, Z., 2016. Perspectives on monitoring gradual change across the continuity of Landsat sensors using time-series data. Remote Sens. Environ. 185, 258–270.
Wang, J., Liu, D., Ciais, P., Peñuelas, J., 2022b. Decreasing rainfall frequency contributes to earlier leaf onset in northern ecosystems. Nat. Clim. Chang. 12 (4), 386–392.
Wang, Z., Jiang, R., Xue, H., Salim, F.D., Song, X., Shibasaki, R., 2022, June. Event-aware multimodal mobility nowcasting. In: Proceedings of the AAAI Conference on Artificial Intelligence, vol. 36(4), pp. 4228–4236.
White, J.C., Wulder, M.A., Hermosilla, T., Coops, N.C., Hobart, G.W., 2017. A nationwide annual characterization of 25 years of forest disturbance and recovery for Canada using Landsat time series. Remote Sens. Environ. 194, 303–321.
Wu, Q., Lane, C.R., Li, X., Zhao, K., Zhou, Y., Clinton, N., DeVries, B., Golden, H.E., Lang, M.W., 2019. Integrating LiDAR data and multi-temporal aerial imagery to map wetland inundation dynamics using Google earth engine. Remote Sens. Environ. 228, 1–13.
Wulder, M.A., Masek, J.G., Cohen, W.B., Loveland, T.R., Woodcock, C.E., 2012. Opening the archive: how free data has enabled the science and monitoring promise of Landsat. Remote Sens. Environ. 122, 2–10.
Wulder, M.A., White, J.C., Loveland, T.R., Woodcock, C.E., Belward, A.S., Cohen, W.B., Fosnight, E.A., Shaw, J., Masek, J.G., Roy, D.P., 2016. The global Landsat archive: status, consolidation, and direction. Remote Sens. Environ. 185, 271–283.
Ye, S., Rogan, J., Zhu, Z., Hawbaker, T.J., Hart, S.J., Andrus, R.A., Meddens, A.J., Hicke, J.A., Eastman, J.R., Kulakowski, D., 2021. Detecting subtle change from dense Landsat time series: case studies of mountain pine beetle and spruce beetle disturbance. Remote Sens. Environ. 263, 112560.
Zeng, Y., Hao, D., Park, T., Zhu, P., Huete, A., Myneni, R., Knyazikhin, Y., Qi, J., Nemani, R.R., Li, F., Huang, J., 2023. Structural complexity biases vegetation greenness measures. Nature Ecology & Evolution 7 (11), 1790–1798.
Zeng, H., Jia, G., Forbes, B.C., 2013. Shifts in Arctic phenology in response to climate and anthropogenic factors as detected from multiple satellite time series. Environ. Res. Lett. 8 (3), 035036.
Zhang, C., Song, D., Chen, Y., Feng, X., Lumezanu, C., Cheng, W., Ni, J., Zong, B., Chen, H., Chawla, N.V., 2019. A deep neural network for unsupervised anomaly detection and diagnosis in multivariate time series data. In: Proceedings of the AAAI Conference on Artificial Intelligence, vol. 33(1), pp. 1409–1416.
Zhang, Y., Woodcock, C.E., Chen, S., Wang, J.A., Sulla-Menashe, D., Zuo, Z., Olofsson, P., Wang, Y., Friedl, M.A., 2022. Mapping causal agents of disturbance in boreal and arctic ecosystems of North America using time series of Landsat data. Remote Sens. Environ. 272, 112935.
Zhao, K., Jackson, R.B., 2014. Biophysical forcings of land-use changes from potential forestry activities in North America. Ecol. Monogr. 84 (2), 329–353.
Zhao, K., Suarez, J.C., Garcia, M., Hu, T., Wang, C., Londo, A., 2018. Utility of multitemporal lidar for forest and carbon monitoring: tree growth, biomass dynamics, and carbon flux. Remote Sens. Environ. 204, 883–897.
Zhao, K., Wulder, M.A., Hu, T., Bright, R., Wu, Q., Qin, H., Li, Y., Toman, E., Mallick, B., Zhang, X., Brown, M., 2019. Detecting change-point, trend, and seasonality in satellite time series data to track abrupt changes and nonlinear dynamics: a Bayesian ensemble algorithm. Remote Sens. Environ. 232, 111181.
Zhong, R., Yan, K., Gao, S., Yang, K., Zhao, S., Ma, X., Zhu, P., Fan, L., Yin, G., 2024. Response of grassland growing season length to extreme climatic events on the Qinghai-Tibetan plateau. Sci. Total Environ. 909, 168488.
Zhu, Z., 2017. Change detection using Landsat time series: a review of frequencies, preprocessing, algorithms, and applications. ISPRS J. Photogramm. Remote Sens. 130, 370–384.
Zhu, Z., Woodcock, C.E., 2014. Continuous change detection and classification of land cover using all available Landsat data. Remote Sens. Environ. 144, 152–171.
Zhu, Z., Zhang, J., Yang, Z., Aljaddani, A.H., Cohen, W.B., Qiu, S., Zhou, C., 2020. Continuous monitoring of land disturbance based on Landsat time series. Remote Sens. Environ. 238, 111116.
Zhu, Z., Qiu, S., Ye, S., 2022. Remote sensing of land change: a multifaceted perspective. Remote Sens. Environ. 282, 113266.